Review Article

Technical principles, benefits, challenges, and applications of photon counting computed tomography in coronary imaging: a narrative review

Antonella Meloni[1,2], Erica Maffei[3], Vincenzo Positano[1,2], Alberto Clemente[2], Carmelo De Gori[2], Sergio Berti[4], Ludovico La Grutta[5], Luca Saba[6], Eduardo Bossone[7], Cesare Mantini[8], Carlo Cavaliere[3], Bruna Punzo[3], Simona Celi[9], Filippo Cademartiri[2]

[1]Bioengineering Unit, Fondazione G. Monasterio CNR-Regione Toscana, Pisa, Italy; [2]Department of Radiology, Fondazione G. Monasterio CNR-Regione Toscana, Pisa, Italy; [3]Department of Radiology, IRCCS SYNLAB SDN, Naples, Italy; [4]Diagnostic and Interventional Cardiology Department, Fondazione G. Monasterio CNR-Regione Toscana, Massa, Italy; [5]Department of Health Promotion, Mother and Child Care, Internal Medicine and Medical Specialties - ProMISE, University of Palermo, Palermo, Italy; [6]Department of Radiology, University Hospital of Cagliari, Monserrato (CA), Italy; [7]Department of Cardiology, Antonio Cardarelli Hospital, Naples, Italy; [8]Department of Radiology, "G. D'Annunzio" University, Chieti, Italy; [9]Bioengineering Unit, Fondazione G. Monasterio CNR-Regione Toscana, Massa, Italy

Contributions: (I) Conception and design: A Meloni, E Maffei, F Cademartiri; (II) Administrative support: A Meloni, V Positano, F Cademartiri; (III) Provision of study materials or patients: E Maffei, A Clemente, C De Gori, S Berti, F Cademartiri; (IV) Collection and assembly of data: A Meloni, E Maffei, L La Grutta, L Saba, E Bossone, C Mantini, C Cavaliere, B Punzo, S Celi, F Cademartiri; (V) Data analysis and interpretation: All authors; (VI) Manuscript writing: All authors; (VII) Final approval of manuscript: All authors.

Correspondence to: Prof., Dr. Filippo Cademartiri, MD, PhD. Department of Radiology, Fondazione G. Monasterio CNR-Regione Toscana, Via Moruzzi, 1 - 56124 Pisa, Italy. Email: fcademartiri@ftgm.it.

Background and Objective: The introduction of photon-counting computed tomography (PCCT) represents the most recent groundbreaking advancement in clinical computed tomography (CT). PCCT has the potential to overcome the limitations of traditional CT and to provide new quantitative imaging information. This narrative review aims to summarize the technical principles, benefits, and challenges of PCCT and to provide a concise yet comprehensive summary of the applications of PCCT in the domain of coronary imaging.

Methods: A review of PubMed, Scopus, and Google Scholar was performed until October 2023 by using relevant keywords. Articles in English were considered.

Key Content and Findings: The main advantages of PCCT over traditional CT are enhanced spatial resolution, improved signal and contrast characteristics, diminished electronic noise and image artifacts, lower radiation exposure, and multi-energy capability with enhanced material discrimination. These key characteristics have made room for improved assessment of plaque volume and severity of stenosis, more precise assessment of coronary artery calcifications, also preserved in the case of a reduced radiation dose, improved assessment of plaque composition, possibility to provide details regarding the biological processes occurring within the plaque, enhanced quality and accuracy of coronary stent imaging, and improved radiomic analyses.

Conclusions: PCCT can significantly impact diagnostic and clinical pathways and improve the management of patients with coronary artery diseases (CADs).

Keywords: Photon-counting detectors; computed tomography angiography (CT angiography); coronary arteries

Submitted Jan 29, 2024. Accepted for publication Jun 27, 2024. Published online Jul 31, 2024.
doi: 10.21037/cdt-24-52
View this article at: https://dx.doi.org/10.21037/cdt-24-52

Introduction

Background

Coronary artery disease (CAD) is a significant global health concern and a leading cause of morbidity and mortality (1). The accurate quantification of CAD extent and severity is a cornerstone of effective CAD management, enabling risk-stratifying patients, selecting the most appropriate treatment approach, and monitoring the patient's progress and the efficacy of the selected therapeutic intervention.

Since its introduction in the 1990s, coronary computed tomographic angiography (CCTA) has evolved as a valuable and increasingly utilized diagnostic tool for detecting and ruling out CAD (2). Indeed, computed tomography (CT) is a non-invasive and widely available imaging technique that offers rapid image acquisition, a broad field of view, and excellent spatial and temporal resolution (3). CCTA has demonstrated high diagnostic accuracy and negative predictive value compared to invasive coronary angiography (ICA), representing the gold standard for assessing CAD (4-7). With the current new-generation CT scanners, high diagnostic accuracy in detecting CAD can also be maintained in patients showing high and/or irregular heart rates (8). Large clinical trials have demonstrated that CCTA was similar to or more effective than functional testing, standard care, or ICA in managing CAD and reducing major adverse cardiovascular events in patients with stable chest pain (9-12). The pivotal role of CCTA in contemporary clinical practice has been reflected in several guidelines (13,14).

Thanks to its ability to look at both the wall and the lumen of the coronary artery, CCTA, besides defining coronary anatomy and luminal stenosis severity, can also provide information on atherosclerotic plaque morphology and composition (15,16). Intravascular ultrasound (IVUS) represents the current gold standard for this purpose (17), but is highly invasive. Several studies performing a head-to-head comparison of CCTA with IVUS confirmed that CCTA, which offers the advantage of being non-invasive, had good diagnostic accuracy in quantifying plaque volumes and identifying adverse plaque characteristics (18-21).

Like any medical imaging technique, conventional CT faces certain critical challenges. Compared to invasive methods, CT has inherent limitations in spatial and temporal resolution and may be less appropriate for high-risk patients presenting with dense calcifications, multiple or small-diameter stents, and irregular heart rhythms (22,23). From a patient safety perspective, the main concerns are the increased risk of cancer due to radiation and the administration of iodinated contrast agents, which can cause allergic reactions and be problematic for patients with impaired renal function (24).

Rationale and knowledge gap

Photon-counting computed tomography (PCCT) represents the most recent breakthrough in clinical X-ray imaging. It harbors the potential to overcome many of the limitations and shortcomings of current CT systems (25,26). Indeed, thanks to the distinct approach to X-ray detection, photon counting detectors (PCDs) present a plethora of advantages over energy-integrating detectors (EIDs) employed in traditional CT scanners (27-30).

Objective

This narrative review aims to summarize the technical principles, benefits, and challenges of PCCT, to provide a concise yet comprehensive summary of the applications of PCCT in coronary imaging, and to illustrate with case examples how this cutting-edge technology may translate into improved clinical diagnosis. We present this article in accordance with the Narrative Review reporting checklist (available at https://cdt.amegroups.com/article/view/10.21037/cdt-24-52/rc).

Methods

PubMed, Scopus, and Google Scholar electronic databases were searched from origin to October 2023. Original research, technical notes, review articles, and guidelines/expert consensus in English were included.

The search strategy is summarized in *Table 1*.

Conventional versus photon-counting detectors

Conventional EIDs use a two-step process to convert X-ray photons into electrical signals (26). The first step involves transforming X-ray photons into visible light via a scintillating material. In the second step, the visible light emitted by the scintillator is captured by an array of photodiodes and converted into electrical impulses. EIDs incorporate optically opaque partitions called septa to separate the cells to avoid optical cross-talk. These layers are approximately 0.1 mm thick and decrease the geometric dose efficiency of the detector because the detected signal

Table 1 The search strategy summary

Items	Specification
Date of search	October 2, 2023
Databases and other sources searched	PubMed, Scopus, and Google Scholar
Search terms used	Photon-counting computed tomography, PCCT, photon counting detector, photon counting X-ray detectors, photon counting CT, spectral CT
Timeframe	No time limit
Inclusion	Original research, technical notes, review articles, and guidelines/expert written in English
Selection process	A.M. analyzed the scientific papers to extract the relevant data for the purpose of this work

PCCT, photon-counting computed tomography; CT, computed tomography.

is not influenced by the X-ray quanta that are absorbed in these areas (31-33). To maintain an acceptable level of signal loss caused by these "dead zones", it becomes impractical to reduce the active detector elements' size. This limitation ultimately constrains the spatial resolution achievable with scintillating detectors. To quantify the energy of all X-ray photons collected during a specific timeframe, the detector combines their signals, and the information about the energy of individual X-ray photons is lost.

PCDs utilize a direct conversion approach (34,35) (*Figure 1*). They are made of semiconductors such as cadmium telluride, cadmium zinc telluride, or silicon (36). A high voltage, typically between 800 and 1,000 V, is applied between the cathode situated on the top side and the pixelated anode electrodes on the bottom side, creating a strong electric field. The interaction between the incident X-ray photon and the detector produces a charge cloud of electron-hole pairs. Under the influence of the electric field, the charge cloud moves towards the anodes and induces short current pulses. An electronic pulse-shaping circuit amplifies and transforms the current pulses into voltage pulses (33). The height of the shaped pulses is proportional to the energy of the absorbed X-rays. A "counter" quantifies the pulses with wave heights exceeding a predetermined energy threshold. By comparing all pulses with multiple energy thresholds, PCDs can categorize the incident photons into various energy groups or bins, allowing for the distinction of X-ray photons according to their energy levels (33). The energy bins in contemporary PCD CT systems typically range from 2 to 8. The width and the number of the energy bins impact the image quality (37,38). Conventionally, the first threshold is set higher than the background noise level of the detector and the other thresholds are either uniformly spaced or strategically chosen to optimize performance for specific tasks.

Advantages of PCCT

Increased spatial resolution

The properties of the detector, including pixel size and scattering characteristics, affect the spatial resolution of a CT scan.

In recent years, the spatial resolution of EIDs has improved, and pixel pitches have now reached approximately 0.5 mm at the detector (39). However, the current dimensions of EID pixels cannot be significantly reduced beyond their current size without a decline in dose efficiency (40). On the other side, the septa cannot be made excessively thin to avoid photon cross-talk, which can compromise the quality of the image. Improving the spatial resolution of scintillator detectors, for example, using a dedicated attenuating filter decreasing the pixel aperture (41), causes a notable rise in radiation dose.

PCDs enable for reduction in pixel size without sacrificing geometric efficiency because there are no non-responsive regions in between the pixels (40). The pixel pitch can be as fine as 0.15–0.225 mm at the isocenter (42-45). Achieving this requires a corresponding small focal spot in the X-ray tube, even if it reduces tube power.

Improved contrast

In EIDs, the quanta with lower X-ray energy levels emit comparatively less light than those with higher energy levels. As a result, the contribution of low-energy X-rays to the total detector signal is reduced. PCDs quantize all X-ray

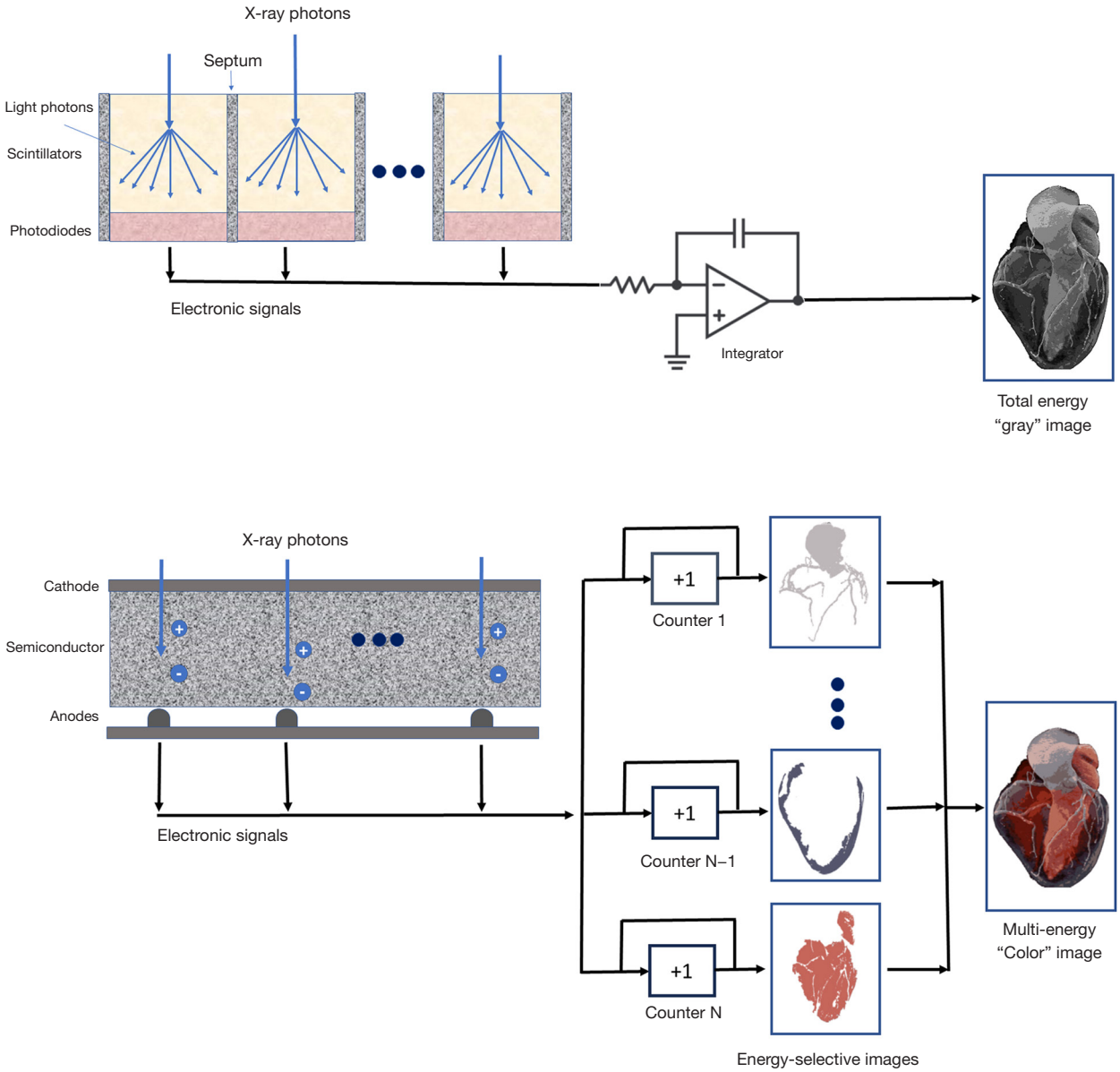

Figure 1 Schematic representation of an energy integrating detector (top) and of a photon-counting detector that directly converts X-rays into electrical signals (bottom). In the photon-counting detector, the interaction between the incident X-ray photon and the semiconductor generates a cloud of positive and negative charges, which pull away from each other under the influence of the electric field. As the electrons reach the anodes, they generate short current pulses, which are converted into voltage pulses. The detector's electronics analyzes the pulses by comparing their amplitudes (proportional to the photon's energy) with predefined threshold levels.

quanta possessing an energy greater than a predetermined minimum energy threshold with uniform weighting. Therefore, low-energy X-ray quanta have equal importance in contributing to the detector signal as their higher-energy counterparts (33,40,46). Since the information about the contrast between different materials is concentrated within the low X-ray energy range, the PCD-CT technology offers improved contrast and contrast-to-noise ratio (CNR) compared to traditional EID-CT, especially for materials with low X-ray attenuation, like iodine (36,47-49). The difference in iodine contrast between PCD-CT and EID-CT is more pronounced as the X-ray tube voltage increases.

In EIDS, the increased variance relative to the mean value, caused by a non-uniform weighting of photons, can result in a reduced signal-to-noise ratio (SNR). PCDs eliminate this phenomenon and its negative effects on image quality.

Elimination of electronic noise

In PCDs, only X-ray photons surpassing an energy threshold of approximately 20–25 keV are registered. This threshold is considerably higher than the electrical system's background noise level. Consequently, electronic noise has not effect on PCDs count rates (33).

Mitigating electronic noise enhances image quality for low-dose scans and scans of patients with large body sizes. In these specific contexts, PCDs have demonstrated their capability to reduce streak artifacts, enhance the uniformity of the imaging signal, and deliver more consistent CT numbers compared to conventional EIDs (50-52).

Multi-energy acquisition

Spectral CT goes beyond traditional CT scanning. It uses different energy levels of X-rays to gather detailed information about the composition and characteristics of tissues within the body and about the spatial and temporal distributions of the contrast agents, enabling better differentiation between materials, improved tissue contrast, and potentially more accurate diagnoses.

Material decomposition is the basis for spectral CT imaging. The different base materials within an imaged area are separated and quantified based on their distinct X-ray attenuation characteristics at different energy levels. The number (N) of detectable base materials corresponds to the number of acquired spectral data points. The material decomposition in N+1 bases with measurements at N different energies is possible. However, it requires the use of supplemental constraints, such as having one material with different spectral behavior, assuming volume or mass conservation, or employing precalibrated subregions in the low- and high-energy space (53). These constraints may introduce inaccuracies in the material decomposition process (54).

Conventional EID-based dual-energy CT (DECT) acquires data in two energy regimes. DECTs are divided into two major groups based on how the two different X-ray energies are generated: source-based and detector-based (55-57). Source-based DECT involves acquiring CT measurements at two different energy spectra. It includes: (I) dual-spin mode in which two scans are performed sequentially by a single X-ray tube and the resulting images overlap; (II) dual-source (DS) mode which involves the use of two orthogonal X-ray tubes operating at different kilovoltages to achieve precise spectral separation and the co-registration of the two acquired images datasets; (III) rapid kVp switching mode in which a single X-ray tube rapidly changes kilovoltage during scanning; and (IV) twin-beam mode in which a single X-ray spectrum is divided into two distinct energy spectra through pre-filtration methods. In detector-based DECT (dual-layer DECT), the energy separation takes place at the detector level due to the scanner's configuration, which includes a single X-ray source and a multilayer detector. Every layer is designed to maximize sensitivity to particular photon energies: the top layer preferentially absorbs low-energy photons while the bottom layer absorbs the high-energy photons.

DECT can distinguish between up to three types of materials within the imaged region (53). Furthermore, DECT suffers from spectral overlap, which reduces the accuracy of material decomposition. PCDs, due to their capability of distinguishing photons with varying energies via pulse-height analysis, offer multi-energy spectral CT without spectral overlap (58) and have the potential for accurate discrimination of ≥3 materials (59). Conversely to DECT based on DS or rapid tube potential switching, PCCT data are inherently acquired at constant tube potential, and there is perfect temporal alignment of the different energy images (60). The material decomposition leads to the creation of material-specific images which provide a clear and detailed representation of the spatial distribution and concentration of a particular material within the region of interest. Post-processing algorithms can also generate virtual non-contrast (VNC) images, where the effects of the administered contrast agent are removed, serving the very important purpose to eliminate the need for acquisition of true non-contrast (TNC) images and save radiation dose, or iodine-specific images, which map the spatial distribution and concentration of iodine-based contrast agents within the scanned region (61-65). Moreover, the energy-independent information can be used to generate synthetic monoenergetic images, which are also referred to as virtual monoenergetic or monochromatic images (VMIs) (66-70). VMIs simulate the appearance of images obtained with a monochromatic X-ray source. Low-energy VMIs are used to improve the enhancement of iodinated contrast and contrast-to-noise-ratio, enabling a

reduction in contrast agent volume, while VMIs at higher energy levels (above 70 keV) are used to minimize artifacts.

The X-ray energy discrimination capabilities inherent to PCDs enable the realization of K-edge imaging, that is, the detection and quantification of elements with a K-edge in the diagnostic energy range. This is achieved by customizing the acquisition energy thresholds to catch the distinct energy shifts at the K-edge of the target materials (71). Different materials with high atomic numbers, besides iodine, can be identified based on their unique K-edge signatures. Typical elements with physical and toxicological properties suitable for human use are tantalum, tungsten, gold, bismuth, gadolinium, and ytterbium (59,72,73). The possibility to differentiate between multiple contrast agents clears the path for multi-material imaging and molecular imaging (74-77). Multi-material imaging can be used to capture the specific distribution of various contrast agents administered concurrently or to image at a single time point multiple contrast agents with different distribution properties (32,46). Capturing multiple contrast phases in a single scan acquisition reduces the radiation dose by eliminating the need for multi-phase CT scans. It allows for perfect spatial alignment between the different phases (78). Dual-contrast CT protocols can potentially furnish datasets rich in features and functional information. Molecular imaging provides real-time visualization of cellular functions of living organisms and related molecular interactions, providing information that cannot be achieved with anatomical and functional imaging (79). Molecular CT imaging may exploit the K-edge imaging to detect targeted contrast agents, that is, contrast agents conjugated with nanoparticles that enable interactions with a target (cells or enzymes) (80-83).

Artifact reduction

Beam hardening is one of the most observed physical-based types of artifacts. Beam hardening artifacts arise due to the uneven attenuation of X-ray beams as they traverse an object. High-density materials absorb X-rays more readily than low-density materials such as water or its related substances. This disparity in attenuation leads to distortions in the reconstructed CT images, presenting as streaking or shading artifacts (84). In PCDs, constant weighting enables the normalization of attenuation measurements across various energy levels, effectively mitigating the impact of beam hardening (85). The high-energy-bin image in PCCT is less susceptible to the distortions caused by beam hardening than low-energy PCCT (34,86).

PCDs have demonstrated significant advantages in mitigating calcium-blooming and metal artifacts, resulting from volume averaging, motion during scanning, and beam-hardening effects. This is achieved through enhanced spatial resolution, which reduces partial volume effects, and improved material decomposition techniques, which allow for the accurate differentiation between high-density materials like metals and surrounding soft tissues (34,87).

The outstanding temporal resolution and precise spatial alignment between the low and high-energy images achievable with PCCT pave the way for creating iodine maps resistant to motion artifacts. In a phantom study, the DS PCCT system proved effective in freezing motion artifacts, while the DS DECT system, with its slower 125 ms temporal resolution, experienced more pronounced motion artifacts (88).

Issues of PCCT

Technical issues

The performance of PCDs can be affected by different physical effects, including cross talk due to charge sharing, K-fluorescence, Compton scattering, and pulse pile-up (31,33,89).

Charge sharing takes place when the charge cloud arrives near the boundary between pixels and is detected by multiple neighboring pixel electrodes (71,90,91). The charge may be erroneously assigned to multiple pixels instead of being accurately allocated to just one pixel (92). Secondary photons resulting from processes like Compton scattering and fluorescence within the detector can be detected in neighboring pixels, leading to the occurrence of multiple events sharing the total energy of the incident photon (33). K-fluorescence is more likely to occur in detectors with higher atomic numbers (cadmium telluride), while the effects of Compton scattering are more pronounced in silicon detectors (32). Collectively, these effects give rise to several issues, including inaccurate assignment of energy to a pixel, undercounts or overcounts, reduced spatial resolution caused by the distribution of counts across neighboring pixels, and correlations between energy bins in different pixels (71). Since the likelihood of charge sharing and cross-talk from secondary photons increases as pixels become smaller, these effects impose a practical constraint on the minimum pixel size obtained in PCDs.

Pulse pile-up occurs when two X-ray photons hit the

detector within the detector's readout time window. This overlap can result in a single, combined pulse that contains information from multiple photons (93). The introduced errors in both photon counting and energy measurement can lead to distorted energy spectra and compromised image quality. The pulse pile-up can be mitigated by reducing the pixel size of the detector, thereby reducing the number of incident photons per detector channel. Anyway, the impact of pulse pile-up is insignificant under the typical X-ray flux rates experienced during clinical CT scans (94).

Alternative contrast agents

Certain clinical applications of PCCT employ alternative contrast agents (80,83). Moreover, the use of two contrast media with different pharmacokinetic profiles, distribution volumes, or application routes may further expand the diagnostic capabilities of PCCT by addressing new clinical indications (59,75).

Compared to magnetic resonance imaging, PCCT requires a significantly higher dose of gadolinium (77,95). The increased dosage generates worries regarding patient safety and raises the need to evaluate the risk-benefit ratio carefully.

Contrast agents like gold and bismuth are still experimental and not approved for human examinations.

More studies on alternative contrast agents are needed to assess their safety, effectiveness, and potential benefits over conventional contrast agents.

High cost

The high cost of PCCT systems (3 to 5 times higher compared to conventional CT scanners) presents a major obstacle to their widespread implementation in clinical environments. However, once the technology becomes more established and the downstream improvements in health outcomes and efficiency are clearly proved, a notable reduction in costs is anticipated to take place.

PCCT for coronary imaging

Diagnostic accuracy

Few *in-vivo* studies evaluated the diagnostic accuracy of ultra-high resolution (UHR) PCCT in detecting CAD compared with ICA.

In the multi-center study of Soschynski *et al.*, nine patients underwent both PCCT and ICA for significant CAD detection (stenosis ≥50%) and PCCT showed no false-negative diagnoses and two false-positive diagnoses (96). Considering the 126 coronary segments, the diagnostic performance of PCCT for significant CAD was very high, with sensitivity =92% and specificity =96%. However, the limited sample size impacts the generalizability of these findings.

In another study on 68 high-risk subjects candidate for transcatheter aortic valve replacement, UHR PCCT provided high diagnostic accuracy in CAD detection compared to ICA, with sensitivity and specificity, respectively, of 96% and 84% per participant, 89% and 91% per vessel, and 77% and 95% per segment (97). The accuracy remained high also in the subgroup of patients with severe calcifications (sensitivity =93%; specificity =70%) and prior stent placement (sensitivity =100%; specificity =86%). Similar results were obtained in the study by Eberhard *et al.*, involving 31 patients candidate for transcatheter aortic valve replacement (98). When compared to ICA, UHR PCCT provided accurate quantification of diameter stenoses, with the Bland-Altman analysis showing a mean difference of 0% and limits of agreement between –8% and 8%, as well as accurate stenosis categorization.

Although these findings need to be confirmed by larger studies, they support the use of PCCT as a valid, safe, and non-invasive alternative to ICA.

Coronary lumen detection

Numerous studies have demonstrated how the increased spatial resolution, soft-tissue contrast, and reduced noise achieved with PCCT translate into an improved assessment of plaque volume and severity of stenosis. An early and accurate assessment of stenosis degree is essential for guiding clinical decisions regarding the subsequent course of treatment and determining whether preventive pharmacotherapy or surgical interventions are most appropriate.

In a phantom study, PCCT images [ultra-high-resolution (HR) protocol] demonstrated a 2.3-fold higher detectability index for coronary lumen and a 2.9-fold higher detectability index for non-calcified plaque than EID-CT images (87). This study by Si-Mohamed *et al.* also included a clinical validation phase in which both PCCT and traditional CT angiography were conducted on 14 patients. Three radiologists conducted image processing, confirming that PCCT images had increased image quality and diagnostic

confidence compared to conventional CT images (87).

The *in-vivo* study from Pinos *et al.* demonstrated that PCCT images (polychromatic images and virtual monoenergetic images at 40, 45, 50, 55, 60 and 70 keV) were characterized by superior subjective quality (improved image noise, vessel attenuation, and vessel sharpness) and higher CNR than polychromatic images from conventional CT (99). The relative CNR gain achieved in PCCT was higher in obese patients than in patients with a body mass index (BMI) <30 kg/m^2 (53.1% *vs.* 39.9%), suggesting that PCCT can be particularly beneficial for patients with increased BMIs. In line with these findings, a larger multi-center study involving 92 patients demonstrated that images obtained with PCCT and analyzed by two experienced radiologists were characterized by very high image quality and CNR (96). Furthermore, the detectability of the relevant proximal and mid-coronary segments with a lumen diameter >2 mm was excellent. Yang *et al.* evaluated *in vivo* the influence of different kernels and strength levels on image quality in PCCT with spectral high-pitch mode (100). Reconstructions with the medium sharp kernel (e.g., Bv40) emerged as the most beneficial in terms of both objective image quality (attenuation, noise, CNR, and vessel sharpness) and subjective image quality evaluated using a five-point Likert scale.

PCCT proved particularly beneficial in evaluating luminal stenosis within heavily calcified plaques. Severely calcified plaques can introduce blooming artifacts, which can make the examinations inconclusive or cause an overestimation of stenosis and a generation of false-positive diagnoses, impacting patient care and treatment decisions (101,102). In their phantom study, Koons *et al.* replicated coronary arteries with calcifications of different sizes and shapes and proved that, compared to conventional CT at an equivalent dose, UHR PCCT provided enhanced visualization of calcium plaques and a clearer view of the patent lumen (30). Furthermore, PCCT exhibited superior accuracy in quantifying luminal stenosis across all types of plaques. Notably, for a ring-shaped plaque causing a decrease of 75% in the vessel's cross-sectional area, only PCCT-generated images could reveal the presence of iodine within the lumen, highlighting the distinctive ability of PCCT to identify partial blockages missed by conventional CT scans. The previously mentioned *in-vivo* study conducted by Si-Mohamed *et al.* unveiled a notable decrease in blooming artifacts in calcified coronary plaques when utilizing PCCT images instead of EID-CT images (87). Mergen *et al.* evaluated the impact of reconstruction kernel and matrix size on the feasibility and quality of UHR PCCT images in patients with a high coronary calcium load (103). They found that using an edge-enhancing sharp vascular convolution kernel, a field of view of 200×200 mm^2, and a matrix size of 512×512 pixels guaranteed high-quality images and allowed for a precise delineation of plaque characteristics and vessel lumen. In the *in-vivo* study by Halfmann *et al.* involving 114 patients with known or suspected CAD who underwent PCCT, the UHR reconstructions allowed significantly lower percentages of diameter stenosis for calcified stenoses compared with standard resolutions (104). In addition, UHR PCCT led to reclassification of the 54.4% of patients to a lower Coronary Artery Disease Reporting and Data System category.

Li *et al.* introduced an innovative method for calculating the percentage of stenosis in blood vessels (105). This method depended on the material decomposition of both dual-energy and multiple-energy CT images, obviating the necessity for traditional segmentation techniques. The computer simulations demonstrated that the proposed approach addressed issues like partial volume effects and blooming artifacts. The phantom experiments proved that multiple-energy CT images allowed for accurate and reproducible stenosis measurements and that the four-threshold PCCT approach was more efficient in mitigating measurement inaccuracies than DECT and two-threshold PCCT. Moreover, applying the three-basis-material decomposition on the four-threshold PCCT images resulted in the generation of separate maps representing the distribution of calcium, iodine, and water.

Allmendinger *et al.* introduced a new reconstruction algorithm based on spectral CT data, aimed at removing from the image only the calcified components, generating virtual non-calcium (VNCa) images (106). Their phantom study demonstrated that the algorithm enabled the generation of high-quality images even in the presence of motion across a broad spectrum of heart rates and a significant reduction of blooming artifacts, enhancing image interpretability and accuracy in the evaluation of stenosis. The efficacy and the diagnostic utility of the VNCa algorithm were confirmed by two recent independent *in-vivo* studies, where the patients performed both PCCT and ICA (reference standard). In the study by Mergen *et al.*, involving 30 patients with minimal to moderate coronary stenoses, no difference between the diameters stenoses measured on VNCa images and with ICA was detected, while diameter stenoses were significantly overestimated for VMI images (107). Nishihara *et al.* demonstrated that the VNCa

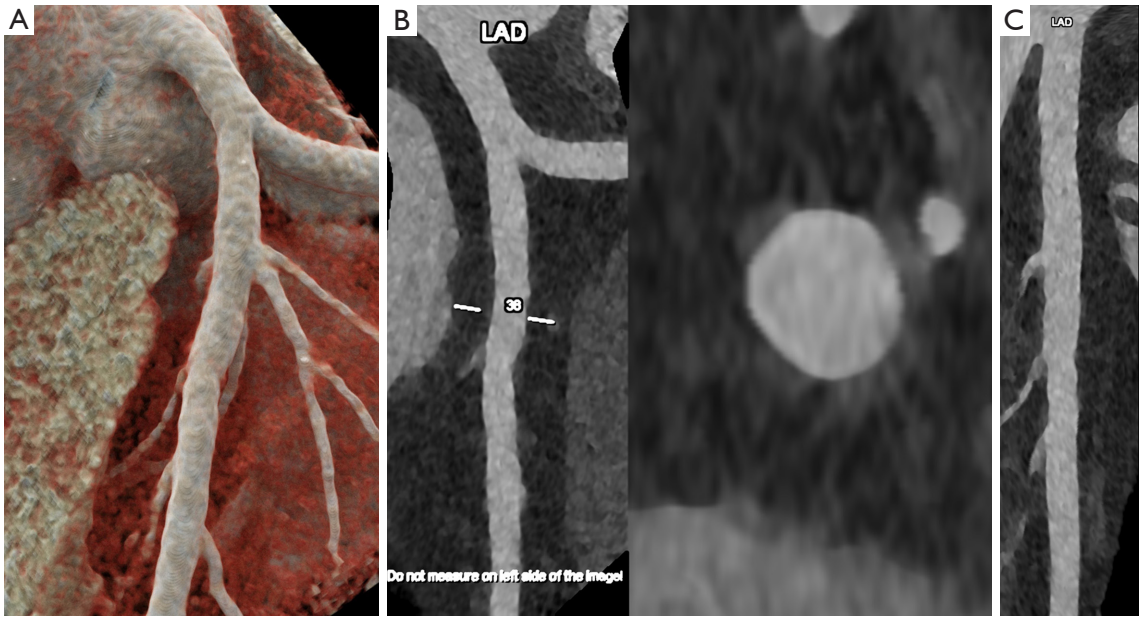

Figure 2 Cardiac/coronary PCCT examples of normal coronary arteries. The figure shows a proximal left coronary artery with 3D cinematic rendering (A), longitudinal MPR and axial cross-section of LAD (B), and longitudinal stretched MPR (C). In this case, coronary arteries are normal (no calcium and no non-calcified atherosclerosis). The scan was performed on a commercial whole-body Dual Source Photon Counting CT scanner (Naeotom Alpha, Siemens Healthineers) with 0.2 mm slice thickness, 0.1 mm reconstruction increment, FOV 140 mm, and IQ level 55. The scan is performed with retrospective ECG gating with tube current modulation and images are displayed with a resolution matrix of 1,024×1,024 pixels on the source axial reconstructions with a kernel filtering of Bv60 (vascular kernel medium-sharp) and with maximum intensity of QIR 4. The actual displayed resolution is 0.1 mm (100 microns). PCCT, photon-counting computed tomography; 3D, three-dimensional; MPR, multiplanar reconstructions; LAD, left anterior descending coronary artery; CT, computed tomography; FOV, field of view; IQ, image quality; ECG, electrocardiogram; QIR, quantum iterative reconstruction.

algorithm improved image interpretability in patients with heavily calcified coronary lesions and the diagnostic accuracy for detecting significant stenosis (≥50%) by ICA over conventional images (108).

Figures 2-9 show examples of coronary PCCT images, including normal coronary arteries (no calcium and no non-calcified atherosclerosis; *Figure 2*), non-obstructive (stenosis <50%) and non-calcified atherosclerosis (*Figure 3*), non-obstructive CAD with calcified lesions (*Figures 4-6*), obstructive CAD (stenosis >50%; *Figures 7,8*), and a high-calcified plaque (Agatston score >1,000; *Figure 9*).

Coronary artery calcium (CAC) score

The CAC score is a reliable marker of atherosclerosis and cardiovascular risk (109,110). Furthermore, it possesses the capacity to function as a screening tool for the detection of occult CAD in asymptomatic individuals, facilitating the implementation of appropriate preventive and treatment strategies (111). The main systems for the quantification of the CAC score are the Agatston method (112), determination of the volume of calcium (113), and determination of the calcium mass score (113), with the Agatston score being the most widely used. In conventional CT scanners, the precision of CAC quantification is impacted by blooming artifacts causing an overestimation of the CAC burden and partial volume effects, which hinder the reliable identification of thin calcifications, resulting in an underestimation of the CAC burden (114,115). PCDs have demonstrated potential to address these challenges.

A phantom study illustrated that, in comparison to conventional EID-CT, PCCT enhanced CAC detection and offered a more precise and accurate quantification of volume scores, particularly when using reduced slice thickness (116). Another phantom study demonstrated the superiority of PCCT over conventional CT in detecting small calcifications, with PCCT emerging able to successfully and accurately detect calcified fragments of 0.4–0.8 mm (117).

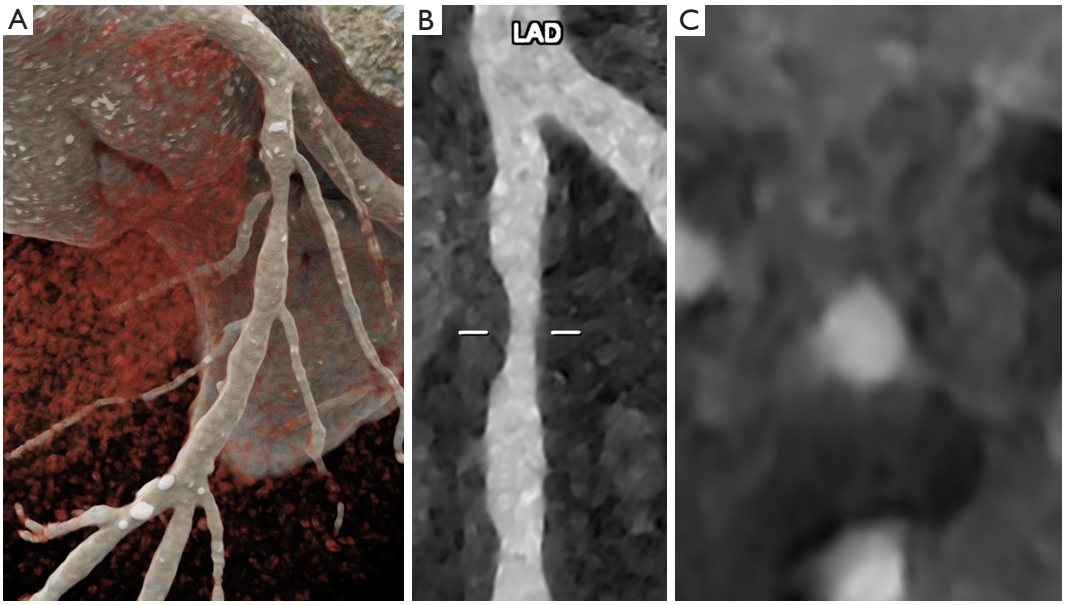

Figure 3 Cardiac/coronary PCCT examples of non-obstructive CAD. In the figure, a proximal left coronary artery is shown with 3D cinematic rendering (A), longitudinal MPR (B), and axial cross-section of LAD (C). In this case, proximal LAD shows predominantly non-calcified atherosclerosis with some positive remodelling. The scan was performed on a commercial whole-body Dual Source Photon Counting CT scanner (Naeotom Alpha, Siemens Healthineers) with 0.2 mm slice thickness, 0.1 mm reconstruction increment, FOV 140 mm, and IQ level 55. The scan is performed with retrospective ECG gating with tube current modulation and images are displayed with a resolution matrix of 1024×1,024 pixels on the source axial reconstructions with a kernel filtering of Bv60 (vascular kernel medium-sharp) and with maximum intensity of QIR 4. The actual displayed resolution is 0.1 mm (100 microns). PCCT, photon-counting computed tomography; CAD, coronary artery disease; 3D, three-dimensional; MPR, multiplanar reconstructions; LAD, left anterior descending coronary artery; CT, computed tomography; FOV, field of view; IQ, image quality; ECG, electrocardiogram; QIR, quantum iterative reconstruction.

An *ex-vivo* study involving cadaveric hearts proved a strong correlation and agreement between the Agatston scores obtained from conventional CT and PCCT and good inter-scan reproducibility for both systems, underscoring the potential of PCCT to become a reliable method for calculating Agatston scores (28). In another *ex-vivo* study, 13 CAC specimens were scanned with conventional EID-CT, UHR PCCT, and micro-CT to create a volume reference standard (118). UHR PCCT showed reduced calcium blooming artifacts and increased accuracy in CAC assessment, leading to a significant reduction in the mean absolute percent error of volume measurements compared to conventional CT (24.1%±25.6% *vs.* 60.1%±48.2%; P<0.01). In their phantom and *in-vivo* study, Eberhard *et al.* showcased the capability of PCCT to quantify CAC burden accurately. They demonstrated that the optimization of the iterative image reconstruction algorithm and the increase in the kilo electron volt levels used for generating VMIs improved CAC assessment's accuracy and reliability (119). Expanding on this research, a study using a dynamic phantom and intermediate monoE levels demonstrated that, when reconstructed at an increased monoE level of 74 or 76 keV PCCT, Agatston scores were in line with the reference conventional CT scores for heart rates of <60 bpm (120). The disparity in the measurements was larger at increasing heart rates.

Before introducing the CAC screening in asymptomatic individuals, it is crucial to balance the potential advantages and drawbacks of exposure to ionizing radiation from recurrent CT scans. The capacity of PCCT to maintain a high degree of sensitivity in detecting CAC while simultaneously reducing radiation exposure was demonstrated by the different phantom studies conducted by van der Werf *et al.* For PCCT acquisitions performed at 90 kVp, monoE reconstructions set at 70 keV enabled consistent and reproducible Agatston scores for medium- and high-density CAC densities while reducing radiation exposure up to 67% (121). The key findings from the study

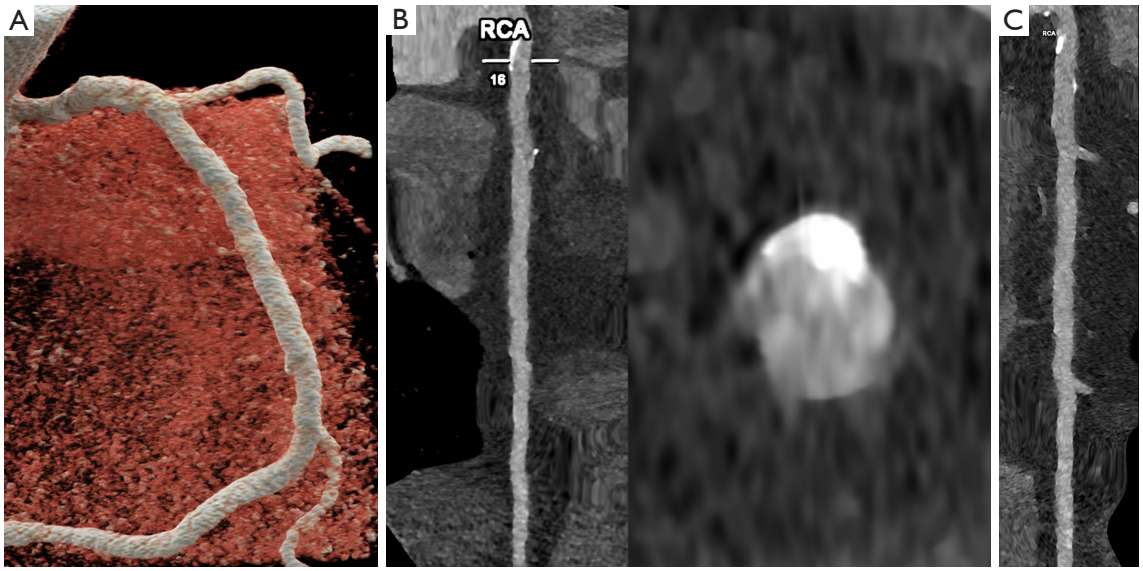

Figure 4 Cardiac/coronary PCCT examples of non-obstructive CAD. In the figure, a complete RCA is shown with 3D cinematic rendering (A), longitudinal MPR and axial cross-section of LAD (B), and longitudinal stretched MPR (C). In this case, proximal RCA shows calcified plaques that do not affect the lumen diameter. The scan was performed on a commercial whole-body Dual Source Photon Counting CT scanner (Naeotom Alpha, Siemens Healthineers) with 0.2 mm slice thickness, 0.1 mm reconstruction increment, FOV 140 mm, and IQ level 55. The scan is performed with retrospective ECG gating with tube current modulation and images are displayed with a resolution matrix of 1,024×1,024 pixels on the source axial reconstructions with a kernel filtering of Bv60 (vascular kernel medium-sharp) and with maximum intensity of QIR 4. The actual displayed resolution is 0.1 mm (100 microns). PCCT, photon-counting computed tomography; CAD, coronary artery disease; RCA, right coronary artery; 3D, three-dimensional; MPR, multiplanar reconstructions; LAD, left anterior descending coronary artery; CT, computed tomography; FOV, field of view; IQ, image quality; ECG, electrocardiogram; QIR, quantum iterative reconstruction.

applying distinct monoE level-specific Agatston score thresholds for CAC scoring on PCCT were that the use of lower monoE levels led to a notable rise in CNR for each CAC density and that, at a 50% reduced radiation dose, the deviations in Agatston scores were non-relevant when using energy levels between 60 and 100 keV for medium-density CAC and between 60 to 120 keV for high-density CAC (122). The comparative study between conventional CT and PCCT demonstrated that PCCT provided a substantial increase in CAC detection, with improvements of up to 156%, even when reducing radiation dose by 50%, and more precise measurements of physical volumes, particularly when using thinner slice thickness and when dealing with high-density CAC deposits (123). In line with these findings, another group demonstrated on ten *ex vivo* human hearts that, at the lowest dose setting of 50 mAs, PCD scans were characterized by a significantly greater reproducibility of CAC scoring than EID scans (124). Moreover, for 10 healthy volunteers, the agreement between CAC scores obtained at the standard dose and those obtained at a low dose was significantly superior when using the PCD system compared to the EID system.

Thanks to its inherent spectral capabilities, PCCT offers the possibility to reconstruct images without the signal of iodinated contrast and, consequently, to remove the need for a non-enhanced scan, mitigating the overall radiation dose burden experienced by the patient. On a clinical PCCT system, Emrich *et al.* evaluated the accuracy of CAC scoring employing a novel virtual non-iodine (VNI) reconstruction method known as PureCalcium (Siemens Healthineers, Erlangen, Germany). PureCalcium implements a series of procedures that intend to subtract iodine and preserve calcium in CT datasets. They compared it with VNC reconstructions, based on decomposition into two base materials (soft tissue and iodine), and TNC acquisitions (125). It is well known that the VNC algorithm underestimates the CAC score, likely due to the underestimation of plaque density and, to a lesser

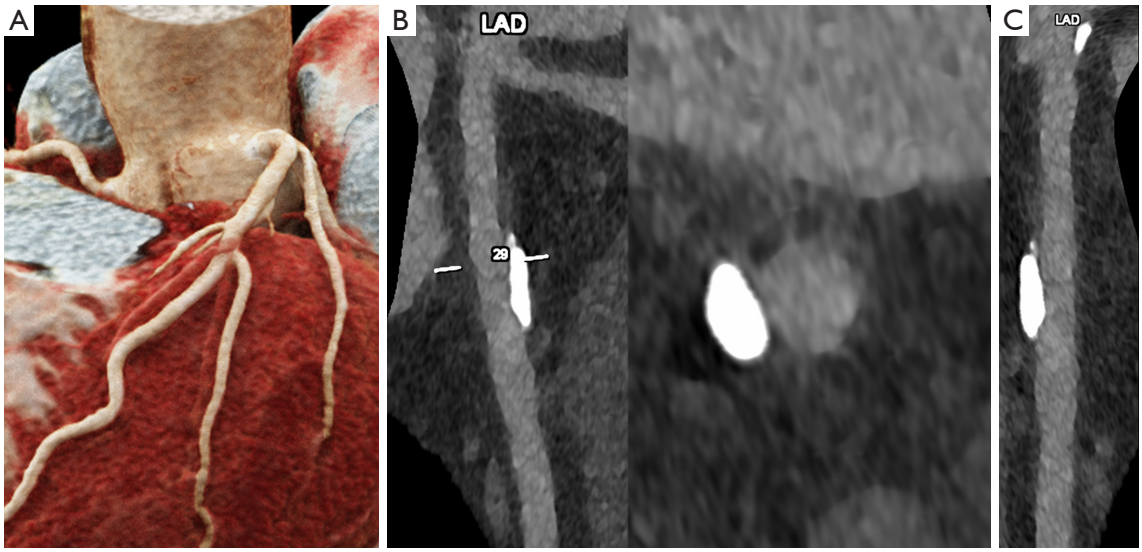

Figure 5 Cardiac/coronary PCCT examples of non-obstructive CAD. In the figure, a proximal left coronary artery is shown with 3D cinematic rendering (A), longitudinal MPR and axial cross-section of LAD (B), and longitudinal stretched MPR (C). In this case, proximal LAD shows a severely calcified plaque that does not affect the lumen diameter; even though the plaque is large, it appears to stay across the coronary artery wall without impacting significantly the lumen diameter. The scan was performed on a commercial whole-body Dual Source Photon Counting CT scanner (Naeotom Alpha, Siemens Healthineers) with 0.2 mm slice thickness, 0.1 mm reconstruction increment, FOV 140 mm, and IQ level 55. The scan is performed with retrospective ECG gating with tube current modulation and images are displayed with a resolution matrix of 1,024×1,024 pixels on the source axial reconstructions with a kernel filtering of Bv60 (vascular kernel medium-sharp) and with maximum intensity of QIR 4. The actual displayed resolution is 0.1 mm (100 microns). PCCT, photon-counting computed tomography; CAD, coronary artery disease; 3D, three-dimensional; MPR, multiplanar reconstructions; LAD, left anterior descending coronary artery; CT, computed tomography; FOV, field of view; IQ, image quality; ECG, electrocardiogram; QIR, quantum iterative reconstruction.

extent, of the underestimation of plaque volume (126). CAC scoring (CACS) PureCalcium and CACS TNC exhibited a strong agreement in the phantom setting. The *in vivo* study involving 67 patients demonstrated that the precision of CACS quantification and the accuracy of CACS classification were notably improved when utilizing PureCalcium reconstructions compared to VNC reconstructions. A recent phantom study evaluating the impact of cardiac motion proved that VNI reconstructions consistently outperformed VNC reconstructions across all heart rates, resulting in a reduced underestimation of CAC scores in comparison to the actual calcium mass and that the Agatston scores obtained from VNI were less influenced by cardiac motion (127). The *in-vivo* study by Mergen *et al.* demonstrated that CAC quantification using VNI images (70 keV) reconstructed from late enhancement scans yielded similar results as compared with TNC images. Moreover, the concordance of CAC risk categories was 97%, with only two patients reclassified to lower risk categories (63).

Coronary plaque characterization

Most acute myocardial infarctions or sudden coronary deaths are triggered by atherosclerotic plaque rupture or erosions leading to vascular thrombosis (128,129). The rupture/erosion-prone atherosclerotic plaques, the so-called "vulnerable plaques" or "high-risk plaques", are characterized by a thin fibrous cap (<65 μm), large necrotic or lipid core, inflammation (in the form of macrophage infiltration), plaque ulceration, intraplaque hemorrhage, spotty calcifications, and expansive vessel remodeling (130). Therefore, the assessment of plaque composition, in addition to plaque burden, can play a pivotal role in improving the prediction of future major adverse cardiovascular events and the tracking of disease progression and response to therapy (131-134).

CCTA performed with the last generation of EID-based systems can be used, combined with dedicated coronary segmentation software, to identify different plaque

Figure 6 Cardiac/coronary PCCT examples of non-obstructive CAD. In the figure, a complete RCA is shown with 3D cinematic rendering (A), longitudinal MPR and axial cross-section of LAD (B), and longitudinal stretched MPR (C). In this case, proximal RCA shows diffuse calcified plaques from the ostium down to crux that do not affect the lumen diameter. The scan was performed on a commercial whole-body Dual Source Photon Counting CT scanner (Naeotom Alpha, Siemens Healthineers) with 0.2 mm slice thickness, 0.1 mm reconstruction increment, FOV 140 mm, and IQ level 55. The scan is performed with retrospective ECG gating with tube current modulation and images are displayed with a resolution matrix of 1,024×1,024 pixels on the source axial reconstructions with a kernel filtering of Bv60 (vascular kernel medium-sharp) and with maximum intensity of QIR 4. The actual displayed resolution is 0.1 mm (100 microns). PCCT, photon-counting computed tomography; CAD, coronary artery disease; RCA, right coronary artery; 3D, three-dimensional; MPR, multiplanar reconstructions; LAD, left anterior descending coronary artery; CT, computed tomography; FOV, field of view; IQ, image quality; ECG, electrocardiogram; QIR, quantum iterative reconstruction.

components based on their diverse X-ray attenuation (135,136). However, with conventional CT systems, some fine characteristics of high-risk plaques cannot be accurately identified, the differentiation of lipid, hemorrhage, and fibrous tissue is problematic, and large calcifications impede the accurate assessment of other plaque constituents (137). PCCT has provided the possibility to overcome these limitations.

The *in-vitro* study conducted by Rotzinger *et al.* compared the performance of PCCT with that of conventional EID-CT under different simulated patient sizes from small to large (138). For all scenarios, the lower noise and higher spatial resolution achievable with PCCT directly translated into improved detection of simulated non-calcified and lipid-rich coronary plaques. Boussel and colleagues imaged with PCCT 10 calcified and 13 lipid-rich non-calcified plaques obtained from post-mortem human coronary arteries (27). By analyzing disparities in spectral attenuation and the concentration of the iodine-based contrast agent, PCCT enabled clear discrimination among normal arterial walls, lipid-rich plaque, calcified areas, and surrounding adipose tissue. The *in-vivo* study by Mergen and colleagues, including 22 coronary plaques from 20 patients, demonstrated that, by mitigating blooming artifacts, implementing the UHR mode in PCCT enabled a more precise and improved visualization of non-calcified plaque constituents (139). Specifically, when compared with reconstructions with the Bv40 kernel and slice thickness of 0.6 mm, used as the reference standard, UHR reconstructions with a slice thickness of 0.2 mm and the Bv64 kernel resulted in a significantly lower volume of calcified components (average difference =32%±7%) and an increased volume of lipid-rich components. Vattay *et al.* assessed in a cohort of 51 patients the effect of VMIs from PCCT on attenuation values and plaque component volumes, employing as reference polychromatic images at

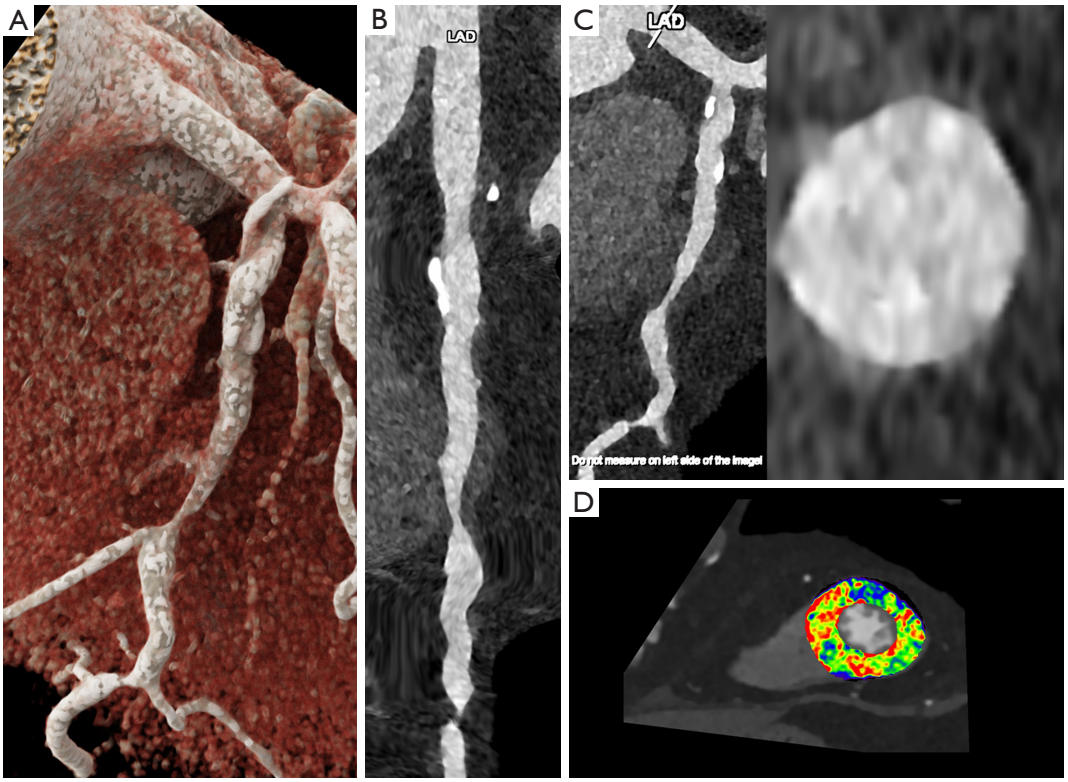

Figure 7 Cardiac/coronary PCCT examples of obstructive CAD. In the figure, a proximal left coronary artery is shown with 3D cinematic rendering (A), longitudinal MPR and axial cross-section of LAD (B), longitudinal stretched MPR (C), and short axis view of the apical segments of the left ventricle first pass rest perfusion map (D). In this case, proximal and middle LAD are severely diseased with predominantly non calcified plaques with positive remodelling and serial significant obstructions of the coronary lumen; the first pass static rest perfusion map shows a perfusion delay (D) at the level of the anterolateral wall of the left ventricle in middle-apical segments (blue colored overlay). The scan was performed on a commercial whole-body Dual Source Photon Counting CT scanner (Naeotom Alpha, Siemens Healthineers) with 0.2 mm slice thickness, 0.1 mm reconstruction increment, FOV 140 mm, and IQ level 55. The scan is performed with retrospective ECG gating with tube current modulation and images are displayed with a resolution matrix of 1,024×1,024 pixels on the source axial reconstructions with a kernel filtering of Bv60 (vascular kernel medium-sharp) and with maximum intensity of QIR 4. The actual displayed resolution is 0.1 mm (100 microns). PCCT, photon-counting computed tomography; CAD, coronary artery disease; 3D, three-dimensional; MPR, multiplanar reconstructions; LAD, left anterior descending coronary artery; CT, computed tomography; FOV, field of view; IQ, image quality; ECG, electrocardiogram; QIR, quantum iterative reconstruction.

120 kVp (T3D) (140). They found that using lower-energy images (40–70 keV) led to an enhancement in the CNR and to an augmented volume of calcified plaque while reducing volumes of non-calcified and lipid-rich plaques. The lowest relative difference compared to T3D images was obtained when using higher VMI levels (100–180 keV) for non-calcified plaque volumes, VMIs at 70 keV for calcified plaque volumes, and low-energy images (40–50 keV) for lipid-rich atheromatous plaque volumes.

The underlying biological mechanisms involved in plaque vulnerability, such as inflammation and neovascularization, can be assessed using molecular imaging techniques. In this context, the new possibilities opened-up by PCCT with K-edge imaging coupled with gold nanoparticles have been demonstrated by both phantom and animal studies. Cormode and colleagues were the first to prove the capability of PCCT to identify macrophages within atherosclerotic lesions while simultaneously visualizing blood vessels and calcified tissue (81). Indeed, on various phantom models and apoE-KO mouse models of atherosclerosis, PCCT could precisely discern among a gold nanoparticle contrast agent targeted at macrophages,

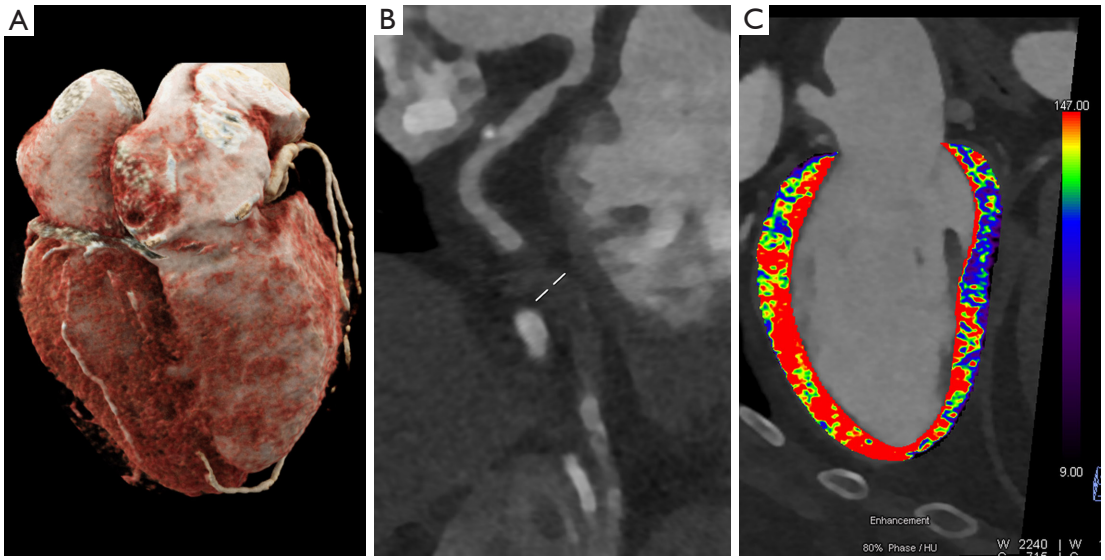

Figure 8 Cardiac/coronary PCCT examples of obstructive CAD. In the figure, a dominant circumflex coronary artery is shown with 3D cinematic rendering (A), longitudinal MPR (B), and two-chamber long axis view of the left ventricle first pass rest perfusion map (C). In this case the middle-distal left circumflex is occluded from a non-calcified plaque; the first pass static rest perfusion map shows a large perfusion delay (C) at the level of the inferior wall of the left ventricle (blue colored overlay). The scan was performed on a commercial whole-body Dual Source Photon Counting CT scanner (Naeotom Alpha, Siemens Healthineers) with 0.2 mm slice thickness, 0.1 mm reconstruction increment, FOV 140 mm, and IQ level 55. The scan is performed with retrospective ECG gating with tube current modulation and images are displayed with a resolution matrix of 1,024×1,024 pixels on the source axial reconstructions with a kernel filtering of Bv60 (vascular kernel medium-sharp) and with maximum intensity of QIR 4. The actual displayed resolution is 0.1 mm (100 microns). PCCT, photon-counting computed tomography; CAD, coronary artery disease; 3D, three-dimensional; MPR, multiplanar reconstructions; LAD, left anterior descending coronary artery; CT, computed tomography; FOV, field of view; IQ, image quality; ECG, electrocardiogram; QIR, quantum iterative reconstruction.

an iodine-based contrast agent, and calcium-rich material. Si-Mohamed *et al.* scanned atherosclerotic and control New Zealand white rabbits both before and 2 days after injecting them with gold nanoparticles and demonstrated an increased association of gold concentration with macrophage for PCCT compared to conventional CT acquisitions (0.82 *vs.* 0.41) (42). Importantly, only PCCT employing gold K-edge imaging could differentiate between the enhancement of the inner lumen with an iodinated contrast agent and the enhancement of the vessel wall with gold nanoparticles. This differentiation was validated through transmission electron microscopy and inductively coupled plasma optical emission spectrometry.

Coronary artery stenting

Coronary artery stent implantation is widely regarded as a safe and well-established technique for treating CAD. Compared to open cardiac surgery, this procedure is minimally invasive and associated with lower mortality and morbidity in the long term and better outcomes in critically ill patients in the short term (141). In-stent restenosis (ISR) arising from neointimal hyperplasia remains one of the main stent-related complications (142). CCTA has emerged as a reliable diagnostic tool for evaluating stented patients, boasting a 98% negative predictive value for excluding significant ISR (143). The 2021 AHA/ACC/ASE/CHEST/SAEM/SCCT/SCMR Guidelines for the Evaluation and Diagnosis of Chest Pain provided a class 2b (moderate) recommendation for the use of CCTA in the assessment of patency of proximal large stents (≥3 mm) (144). With conventional EID-CT scanners, about 8% of stents (thick-strut or small-diameter stents) are not accessible, mostly due to blooming, metallic, and beam-hardening artifacts and reduced spatial resolution (145,146). Several *in-vitro* studies have demonstrated the potential of PCCT to address these issues, improving the quality and accuracy of coronary stent imaging.

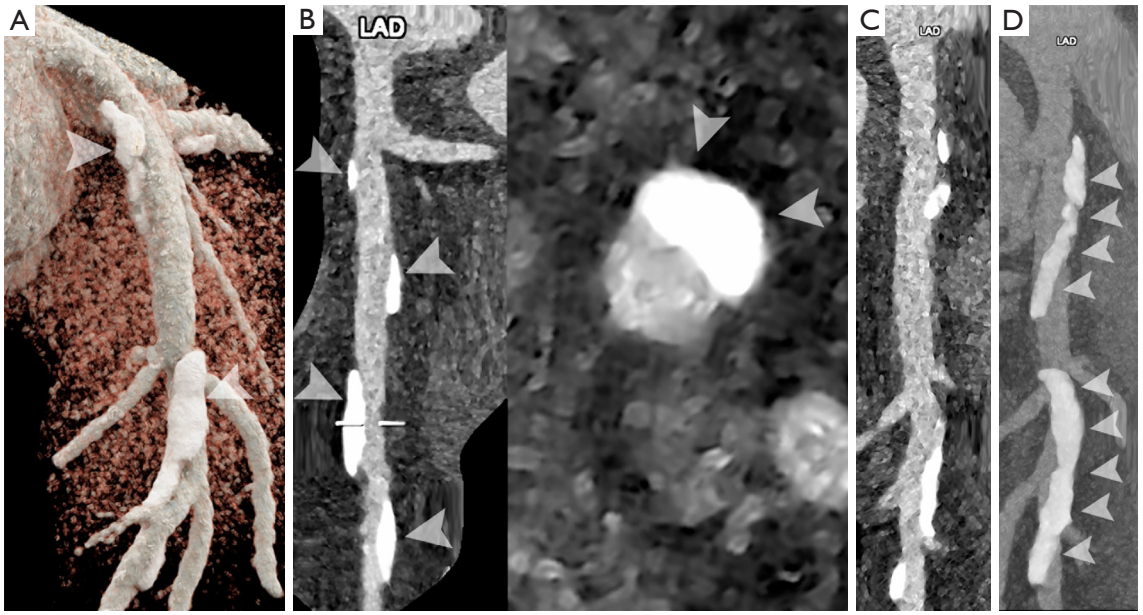

Figure 9 Cardiac/coronary PCCT examples of non-obstructive CAD. In the figure, a proximal left coronary artery is shown with 3D cinematic rendering (A), longitudinal MPR and axial cross-section of LAD (B), longitudinal stretched MPR (C), and longitudinal stretched MIP (D). In this case, proximal-middle LAD shows massively/bulky calcified plaques that, even though very thick and dense, do not significantly affect the lumen diameter (A-D; arrowheads); the Agatston score of the displayed LAD is above 1,000. Technically, the presence of severe calcifications should be approached as the presence of coronary stents. The scan was performed on a commercial whole-body Dual Source Photon Counting CT scanner (Naeotom Alpha, Siemens Healthineers) with 0.2 mm slice thickness, 0.1 mm reconstruction increment, FOV 140 mm, and IQ level 55. The scan is performed with retrospective ECG gating with diastolic tube current modulation and images are displayed with a resolution matrix of 1,024×1,024 pixels on the source axial reconstructions with a kernel filtering of Bv72 (vascular kernel sharp) and with maximum intensity of QIR 4. The actual displayed resolution is 0.1 mm (100 microns). PCCT, photon-counting computed tomography; CAD, coronary artery disease; 3D, three-dimensional; MPR, multiplanar reconstructions; MIP, maximum intensity projection; LAD, left anterior descending coronary artery; CT, computed tomography; FOV, field of view; IQ, image quality; ECG, electrocardiogram; QIR, quantum iterative reconstruction.

In a comparative study where 18 coronary stents made of various material compositions were scanned with both PCCT and conventional CT systems with identical imaging parameters (147), enhanced visibility of the stent lumen, reduced noise levels, decreased occurrence of blooming artifacts, and higher overall image quality were demonstrated for PCCT acquisitions. Different independent studies evaluating the impact of using the UHR mode in PCCT were concordant in reporting superior visibility of the coronary stent lumen and a reduction of metal blooming artifacts for UHR PCCT compared to standard-resolution PCCT and conventional EID-CT (148-152). However, it has been shown that the implementation of a convolutional neural network denoising algorithm to HR PCCT enabled to reduce image noise by about 50% without impacting lumen quantification. Other studies demonstrated that in-stent lumen visibility and sharpness could be improved by using specific sharp reconstruction kernels tailored to the enhanced spatial resolution of PCDs and optimized for stent imaging (151,153,154). Optimized kernels and UHR imaging proved particularly beneficial for stents on a steady phantom with smaller diameters (151).

A complex scenario was considered in the study of Feuerlein *et al.*, where a phantom mimicking a low-density calcified plaque situated within a coronary stent, exhibiting a degree of attenuation similar to the vascular lumen filled with gadolinium, was imaged with a PCCT system with six energy thresholds (155). Thanks to gadolinium K-edge imaging, it was possible to differentiate between intravascular gadolinium-based contrast agent, calcified plaque, and stent material and to effectively suppress beam-hardening artifacts.

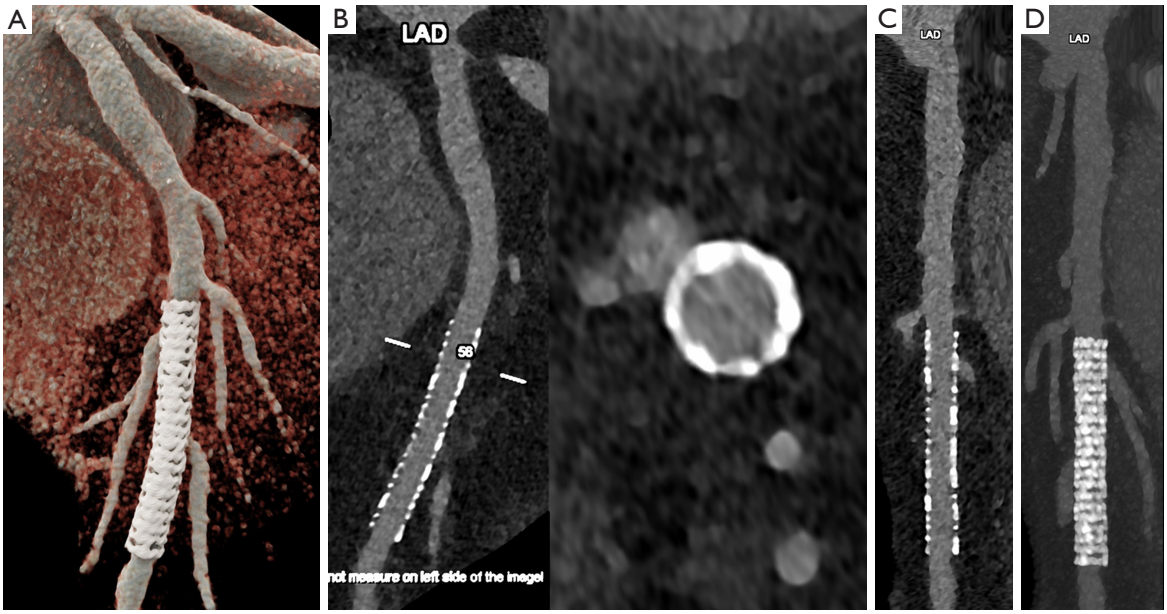

Figure 10 Cardiac/coronary PCCT examples of coronary artery stent. In the figure, it is shown a stent in the mid left anterior descending coronary artery with 3D cinematic rendering (A), longitudinal MPR and axial cross section of coronary lumen within the stent segment (B), stretched MPR (C) and stretched MIP (D). In this case, the stent is perfectly visualized (even the metal stent struts) with perfect visualization of the in-stent lumen. The scan was performed on a commercial whole-body Dual Source Photon Counting CT scanner (Naeotom Alpha, Siemens Healthineers) with 0.2 mm slice thickness, 0.1 mm reconstruction increment, FOV 140 mm, and IQ level 55. The scan is performed with retrospective ECG gating with tube current modulation and images are displayed with a resolution matrix of 1,024×1,024 pixels on the source axial reconstructions with a kernel filtering of Bv72 (vascular kernel sharp) and with maximum intensity of QIR 4. The actual displayed resolution is 0.1 mm (100 microns). PCCT, photon-counting computed tomography; 3D, three-dimensional; MPR, multiplanar reconstructions; LAD, left anterior descending coronary artery; CT, computed tomography; FOV, field of view; IQ, image quality; ECG, electrocardiogram; QIR, quantum iterative reconstruction.

In-vivo human studies have also demonstrated the advantages of PCCT in coronary stent evaluation. In the study by Boccalini *et al.*, where eight patients with coronary stents were scanned using both PCCT and conventional CT, PCCT acquisitions resulted in a lower radiation dose, provided better objective and subjective visibility of both the stent and the coronary lumen, and demonstrated fewer blooming artifacts (156). In the study by Si-Mohamed *et al.*, the PCCT and EID-CT images of eight patients with coronary stents were blindly analyzed by three radiologists who used a five-point scale to measure the diagnostic quality of coronary stents. PCCT was demonstrated to significantly outperform conventional CT, improving overall diagnostic quality by 92% (87). Geering *et al.* assessed the quality of coronary stent lumen visualization with UHR PCCT. They found out that stent struts' sharpness continuously increased at sharper kernels and that in-stent-lumen diameter and attenuation were not influenced by stent angulation (157).

The advantages of PCCT in terms of non-invasive detection of ISR were demonstrated by the *in-vitro* study conducted by Bratke *et al.* (158), where soft-plaque-like stenoses were placed into ten coronary stents embedded in a vessel phantom filled with contrast and imaged with both conventional CT and PCCT. Although both systems effectively identified or suspected the stenosis in all ten stents, the accurate delineation of the residual lumen was feasible for seven stents when utilizing PCCT and never attainable with conventional CT.

Hagar *et al.* compared *in vivo* (44 coronary stents in 18 patients) the accuracy of UHR PCCT versus ICA (reference standard) in assessing coronary stent patency. UHR PCCT demonstrated a diagnostic accuracy for the presence of ISR ≥50% exceeding 88% and a negative predictive value of 100%, emerging as a promising non-invasive alternative to ICA (159).

Figures 10,11 show PCCT examples of coronary artery

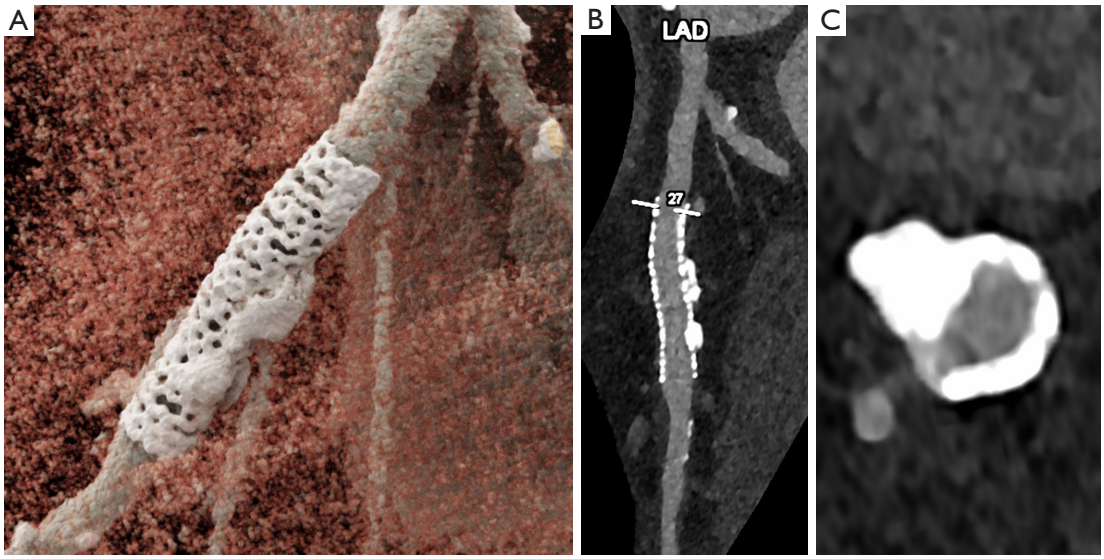

Figure 11 Cardiac/coronary PCCT examples of coronary artery stent. In the figure, it is shown a stent in the proximal left anterior descending coronary artery with 3D cinematic rendering (A), longitudinal MPR (B) and axial cross section of coronary lumen within the stent segment (C). In this case, even though there are some calcifications around the stent, the stent is perfectly visualized (even the metal stent struts) with perfect visualization of the in-stent lumen. The scan was performed on a commercial whole-body Dual Source Photon Counting CT scanner (Naeotom Alpha, Siemens Healthineers) with 0.2 mm slice thickness, 0.1 mm reconstruction increment, FOV 140 mm, and IQ level 55. The scan is performed with retrospective ECG gating with tube current modulation and images are reconstructed and displayed with a resolution matrix of 1,024×1,024 pixels on the source axial reconstructions with a kernel filtering of Bv72 (vascular kernel sharp) and with maximum intensity of QIR 4. The actual displayed resolution is 0.1 mm (100 microns). PCCT, photon-counting computed tomography; 3D, three-dimensional; MPR, multiplanar reconstructions; LAD, left anterior descending coronary artery; CT, computed tomography; FOV, field of view; IQ, image quality; ECG, electrocardiogram; QIR, quantum iterative reconstruction.

stents, demonstrating the perfect visualization of the metal stent struts and the in-stent lumen, even in presence of some calcifications around the stent.

Fractional flow reserve (FFR)

Applying Computational Fluid Dynamics to conventional CCTA data allows to determine the FFR (160,161). CT-derived FFR (CT-FFR) provides a combined anatomic and physiologic evaluation of coronary artery stenosis, allowing enhancement of the specificity of CCTA when evaluating CAD, reducing the occurrence of non-obstructive disease findings during ICA, and playing a crucial role in making informed decisions and plans for revascularization (161,162).

The *in-vivo* study of Zsarnóczay *et al.*, which involved 23 patients, demonstrated a strong agreement between CT-FFR obtained from PCCT and conventional EID-CT acquisitions in the per-vessel analysis and the per-patient analysis (163). A hemodynamically significant CT-FFR (≤0.75) was detected in 10 patients with EID-CT and in nine patients with PCCT.

The *in-vivo* study by Brendel et al, involving 260 patients referred for pre-transcatheter aortic valve replacement work-up, demonstrated that PCCT combined with deep learning models had a good diagnostic accuracy in comparison with ICA for the detection of hemodynamically significant stenosis, defined as invasive FFR ≤0.80 (per-patient sensitivity, specificity, positive predictive value, negative predictive value, and accuracy of 96.8%, 87.3%, 87.8%, 96.7%, and 91.9%, respectively) (164).

Radiomics

Radiomics is a method that involves extracting numerous quantitative features from a medical image, providing detailed descriptions of abnormalities beyond what can be visually assessed by the human eye (165). Key requisites for the extraction of reliable and insightful texture features are high spatial resolution and SNR (166). Therefore, thanks to its associated benefits, PCCT presents the opportunity to

enhance radiomic analyses based on CT imaging data.

In the study by Dunning *et al.*, 19 patients underwent CCTA using PCCT and VMIs at 50, 70, and 100 keV, iodine maps, and VNC images were reconstructed with the goal of assessing how the different image types, by impacting contrast and texture appearance of the coronary plaques, affected the efficacy of coronary plaque risk stratification (167). Ninety-three radiomic features were retrieved from each image and compared between plaques categorized as low- and high-risk by an expert radiologist. The 100 keV VMIs and the VNC images had the highest accuracy in coronary plaque risk classification, due to the decreased presence of iodine and calcium.

Pericoronary adipose tissue (PCAT)

PCAT is the fat deposit surrounding the coronary arteries. PCAT mean attenuation (PCATMA) measurement through CT represents an indirect measure of adipocyte size and lipid content, reflecting inflammation status (168). PCATMA is associated with the severity of stenosis, plaque components, and high-risk plaque features (169-172) and can help in the identification of individuals at increased risk of adverse cardiovascular events, improving the cardiovascular risk stratification beyond the traditional approach, including measurement of coronary calcium and CCTA evaluation (173-175).

Mergen and colleagues evaluated the impact of monoenergetic energy levels on PCAT measurements in 30 patients who underwent CCTA using a first-generation whole-body PCCT system (176). Their findings demonstrated that PCATMA of the right coronary artery, the left anterior descending artery, and the circumflex artery increased with increasing energy levels. They showed significant differences between patients without CAC and with mild CAC at multiple energy levels.

Strengths and limitations

The main strength of this narrative review lies in its comprehensive nature. It provides a technical background of the PCCT technology and highlights its unique features, advantages, and potential limitations, contextualizing PCCT within the broader landscape of medical imaging technologies. Moreover, it synthesizes findings from multiple studies, offering a cohesive overview of the applications of PCCT in coronary imaging and providing insights into its potential impact on patient care and outcomes.

The primary limitation is that, despite our best efforts to encompass the most relevant research, the field of PCCT is continually evolving. Thus, there may be newer findings that were not included in this review. Other limitations encompass potential biases due to the selection of included studies, as well as the reliance on subjective interpretations of the literature. However, every effort has been made to provide a balanced, informative, and rigorous perspective on the topic.

Conclusions

PCCT is based on the direct conversion of X-ray photons into electrical signals and provides a wide range of advantages over traditional CT systems, encompassing improved spatial resolution, better iodine signal, elimination of electrical noise, reduced beam-hardening and metal artifacts, improved dose efficiency, and ability to differentiate multiple intrinsic and contrast materials in a single scan. As demonstrated in phantom, animal and clinical studies, these key features have paved the way for a greatly enhanced CT performance in assessing coronary plaque burden and composition, quantifying coronary calcium, imaging coronary stents, and extracting radiomics features. Although the use of alternative contrast agents has emerged as a promising avenue for enhancing medical imaging, its implementation into clinical routine can be challenging.

Large clinical studies are warranted to unveil the potentialities of PCCT further and prove its ability to improve prognostic stratification and aid in medical decision-making for patients with CAD.

Acknowledgments

The authors gratefully thank all patients whose images were shown in this study.

Funding: None.

Footnote

Reporting Checklist: The authors have completed the Narrative Review reporting checklist. Available at https://cdt.amegroups.com/article/view/10.21037/cdt-24-52/rc

Peer Review File: Available at https://cdt.amegroups.com/article/view/10.21037/cdt-24-52/prf

Conflicts of Interest: All authors have completed the ICMJE uniform disclosure form (available at https://cdt.amegroups.com/article/view/10.21037/cdt-24-52/coif). F.C. and L.S. serve as unpaid editorial board members of *Cardiovascular Diagnosis and Therapy* from September 2023 to August 2025. The other authors have no conflicts of interest to declare.

Ethical Statement: The authors are accountable for all aspects of the work in ensuring that questions related to the accuracy or integrity of any part of the work are appropriately investigated and resolved.

References

1. Brown JC, Gerhardt TE, Kwon E. Risk Factors for Coronary Artery Disease. In: StatPearls. Treasure Island (FL): StatPearls Publishing; January 23, 2023.
2. Serruys PW, Kotoku N, Nørgaard BL, et al. Computed tomographic angiography in coronary artery disease. EuroIntervention 2023;18:e1307-27.
3. Met R, Bipat S, Legemate DA, et al. Diagnostic performance of computed tomography angiography in peripheral arterial disease: a systematic review and meta-analysis. JAMA 2009;301:415-24.
4. Abdulla J, Abildstrom SZ, Gotzsche O, et al. 64-multislice detector computed tomography coronary angiography as potential alternative to conventional coronary angiography: a systematic review and meta-analysis. Eur Heart J 2007;28:3042-50.
5. Budoff MJ, Dowe D, Jollis JG, et al. Diagnostic performance of 64-multidetector row coronary computed tomographic angiography for evaluation of coronary artery stenosis in individuals without known coronary artery disease: results from the prospective multicenter ACCURACY (Assessment by Coronary Computed Tomographic Angiography of Individuals Undergoing Invasive Coronary Angiography) trial. J Am Coll Cardiol 2008;52:1724-32.
6. Miller JM, Rochitte CE, Dewey M, et al. Diagnostic performance of coronary angiography by 64-row CT. N Engl J Med 2008;359:2324-36.
7. Maffei E, Martini C, Tedeschi C, et al. Diagnostic accuracy of 64-slice computed tomography coronary angiography in a large population of patients without revascularisation: registry data in NSTEMI acute coronary syndrome and influence of gender and risk factors. Radiol Med 2011;116:1014-26.
8. Andreini D, Mushtaq S, Pontone G, et al. Diagnostic performance of coronary CT angiography carried out with a novel whole-heart coverage high-definition CT scanner in patients with high heart rate. Int J Cardiol 2018;257:325-31.
9. Douglas PS, Hoffmann U, Patel MR, et al. Outcomes of anatomical versus functional testing for coronary artery disease. N Engl J Med 2015;372:1291-300.
10. SCOT-HEART Investigators, Newby DE, Adamson PD, et al. Coronary CT Angiography and 5-Year Risk of Myocardial Infarction. N Engl J Med 2018;379:924-33.
11. Hoffmann U, Ferencik M, Udelson JE, et al. Prognostic Value of Noninvasive Cardiovascular Testing in Patients With Stable Chest Pain: Insights From the PROMISE Trial (Prospective Multicenter Imaging Study for Evaluation of Chest Pain). Circulation 2017;135:2320-32.
12. DISCHARGE Trial Group; Maurovich-Horvat P, Bosserdt M, et al. CT or Invasive Coronary Angiography in Stable Chest Pain. N Engl J Med 2022;386:1591-602.
13. Knuuti J, Wijns W, Saraste A, et al. 2019 ESC Guidelines for the diagnosis and management of chronic coronary syndromes. Eur Heart J 2020;41:407-77.
14. Writing Committee Members, Gulati M, Levy PD, et al. 2021 AHA/ACC/ASE/CHEST/SAEM/SCCT/SCMR Guideline for the Evaluation and Diagnosis of Chest Pain: A Report of the American College of Cardiology/American Heart Association Joint Committee on Clinical Practice Guidelines. J Am Coll Cardiol 2021;78:e187-e285.
15. Sun Z, Xu L. Coronary CT angiography in the quantitative assessment of coronary plaques. Biomed Res Int 2014;2014:346380.
16. Motoyama S, Ito H, Sarai M, et al. Plaque Characterization by Coronary Computed Tomography Angiography and the Likelihood of Acute Coronary Events in Mid-Term Follow-Up. J Am Coll Cardiol 2015;66:337-46.
17. Stone GW, Maehara A, Lansky AJ, et al. A prospective natural-history study of coronary atherosclerosis. N Engl J Med 2011;364:226-35.
18. Nakazato R, Shalev A, Doh JH, et al. Quantification

and characterisation of coronary artery plaque volume and adverse plaque features by coronary computed tomographic angiography: a direct comparison to intravascular ultrasound. Eur Radiol 2013;23:2109-17.
19. Papadopoulou SL, Neefjes LA, Schaap M, et al. Detection and quantification of coronary atherosclerotic plaque by 64-slice multidetector CT: a systematic head-to-head comparison with intravascular ultrasound. Atherosclerosis 2011;219:163-70.
20. Voros S, Rinehart S, Qian Z, et al. Prospective validation of standardized, 3-dimensional, quantitative coronary computed tomographic plaque measurements using radiofrequency backscatter intravascular ultrasound as reference standard in intermediate coronary arterial lesions: results from the ATLANTA (assessment of tissue characteristics, lesion morphology, and hemodynamics by angiography with fractional flow reserve, intravascular ultrasound and virtual histology, and noninvasive computed tomography in atherosclerotic plaques) I study. JACC Cardiovasc Interv 2011;4:198-208.
21. Lee H, Yoon YE, Lee W, et al. Prognosis of anatomic coronary artery disease without myocardial ischemia: Coronary computed tomography angiography detects high-risk patients even in cases of negative single-photon emission computed tomography findings. J Cardiol 2018;72:162-9.
22. FitzGerald P, Bennett J, Carr J, et al. Cardiac CT: A system architecture study. J Xray Sci Technol 2016;24:43-65.
23. Cademartiri F, Meloni A, Pistoia L, et al. Dual-Source Photon-Counting Computed Tomography-Part I: Clinical Overview of Cardiac CT and Coronary CT Angiography Applications. J Clin Med 2023;12:3627.
24. Rajiah P. Updates in Vascular Computed Tomography. Radiol Clin North Am 2020;58:671-91.
25. Meloni A, Cademartiri F, Pistoia L, et al. Dual-Source Photon-Counting Computed Tomography-Part III: Clinical Overview of Vascular Applications beyond Cardiac and Neuro Imaging. J Clin Med 2023;12:3798.
26. Meloni A, Cademartiri F, Positano V, et al. Cardiovascular Applications of Photon-Counting CT Technology: A Revolutionary New Diagnostic Step. J Cardiovasc Dev Dis 2023;10:363.
27. Boussel L, Coulon P, Thran A, et al. Photon counting spectral CT component analysis of coronary artery atherosclerotic plaque samples. Br J Radiol 2014;87:20130798.
28. Skoog S, Henriksson L, Gustafsson H, et al. Comparison of the Agatston score acquired with photon-counting detector CT and energy-integrating detector CT: ex vivo study of cadaveric hearts. Int J Cardiovasc Imaging 2022;38:1145-55.
29. Polacin M, Templin C, Manka R, et al. Photon-counting computed tomography for the diagnosis of myocardial infarction with non-obstructive coronary artery disease. Eur Heart J Case Rep 2022;6:ytac028.
30. Koons E, VanMeter P, Rajendran K, et al. Improved quantification of coronary artery luminal stenosis in the presence of heavy calcifications using photon-counting detector CT. Proc SPIE Int Soc Opt Eng 2022;12031:120311A.
31. Kreisler B. Photon counting Detectors: Concept, technical Challenges, and clinical outlook. Eur J Radiol 2022;149:110229.
32. Willemink MJ, Persson M, Pourmorteza A, et al. Photon-counting CT: Technical Principles and Clinical Prospects. Radiology 2018;289:293-312.
33. Flohr T, Petersilka M, Henning A, et al. Photon-counting CT review. Phys Med 2020;79:126-36.
34. Leng S, Bruesewitz M, Tao S, et al. Photon-counting Detector CT: System Design and Clinical Applications of an Emerging Technology. Radiographics 2019;39:729-43.
35. Esquivel A, Ferrero A, Mileto A, et al. Photon-Counting Detector CT: Key Points Radiologists Should Know. Korean J Radiol 2022;23:854-65.
36. Iwanczyk JS, Nygård E, Meirav O, et al. Photon Counting Energy Dispersive Detector Arrays for X-ray Imaging. IEEE Trans Nucl Sci 2009;56:535-42.
37. Persson M, Huber B, Karlsson S, et al. Energy-resolved CT imaging with a photon-counting silicon-strip detector. Phys Med Biol 2014;59:6709-27.
38. Zheng Y, Yveborg M, Grönberg F, et al. Robustness of optimal energy thresholds in photon-counting spectral CT. Nuclear Instruments and Methods in Physics Research Section A: Accelerators, Spectrometers, Detectors and Associated Equipment 2020;953:163132.
39. Yanagawa M, Hata A, Honda O, et al. Subjective and objective comparisons of image quality between ultra-high-resolution CT and conventional area detector CT in phantoms and cadaveric human lungs. Eur Radiol 2018;28:5060-8.
40. Danielsson M, Persson M, Sjölin M. Photon-counting x-ray detectors for CT. Phys Med Biol 2021;66:03TR01.
41. Flohr TG, Stierstorfer K, Süss C, et al. Novel ultrahigh resolution data acquisition and image reconstruction for multi-detector row CT. Med Phys 2007;34:1712-23.
42. Si-Mohamed SA, Sigovan M, Hsu JC, et al. In Vivo

Molecular K-Edge Imaging of Atherosclerotic Plaque Using Photon-counting CT. Radiology 2021;300:98-107.
43. Leng S, Rajendran K, Gong H, et al. 150-µm Spatial Resolution Using Photon-Counting Detector Computed Tomography Technology: Technical Performance and First Patient Images. Invest Radiol 2018;53:655-62.
44. Ferda J, Vendiš T, Flohr T, et al. Computed tomography with a full FOV photon-counting detector in a clinical setting, the first experience. Eur J Radiol 2021;137:109614.
45. Rajendran K, Petersilka M, Henning A, et al. First Clinical Photon-counting Detector CT System: Technical Evaluation. Radiology 2022;303:130-8.
46. Sandfort V, Persson M, Pourmorteza A, et al. Spectral photon-counting CT in cardiovascular imaging. J Cardiovasc Comput Tomogr 2021;15:218-25.
47. Shikhaliev PM. Energy-resolved computed tomography: first experimental results. Phys Med Biol 2008;53:5595-613.
48. Shikhaliev PM, Fritz SG. Photon counting spectral CT versus conventional CT: comparative evaluation for breast imaging application. Phys Med Biol 2011;56:1905-30.
49. Silkwood JD, Matthews KL, Shikhaliev PM. Photon counting spectral breast CT: effect of adaptive filtration on CT numbers, noise, and contrast to noise ratio. Med Phys 2013;40:051905.
50. Yu Z, Leng S, Kappler S, et al. Noise performance of low-dose CT: comparison between an energy integrating detector and a photon counting detector using a whole-body research photon counting CT scanner. J Med Imaging (Bellingham) 2016;3:043503.
51. Symons R, Cork TE, Sahbaee P, et al. Low-dose lung cancer screening with photon-counting CT: a feasibility study. Phys Med Biol 2017;62:202-13.
52. McCollough CH, Rajendran K, Leng S. Standardization and Quantitative Imaging With Photon-Counting Detector CT. Invest Radiol 2023;58:451-8.
53. Liu X, Yu L, Primak AN, et al. Quantitative imaging of element composition and mass fraction using dual-energy CT: three-material decomposition. Med Phys 2009;36:1602-9.
54. Yveborg M, Danielsson M, Bornefalk H. Theoretical comparison of a dual energy system and photon counting silicon detector used for material quantification in spectral CT. IEEE Trans Med Imaging 2015;34:796-806.
55. Siegel MJ, Kaza RK, Bolus DN, et al. White Paper of the Society of Computed Body Tomography and Magnetic Resonance on Dual-Energy CT, Part 1: Technology and Terminology. J Comput Assist Tomogr 2016;40:841-5.
56. Tarkowski P, Czekajska-Chehab E. Dual-Energy Heart CT: Beyond Better Angiography-Review. J Clin Med 2021;10:5193.
57. Borges AP, Antunes C, Curvo-Semedo L. Pros and Cons of Dual-Energy CT Systems: "One Does Not Fit All". Tomography 2023;9:195-216.
58. Kappler S, Henning A, Kreisler B, et al. Photon-counting CT at elevated x-ray tube currents: contrast stability, image noise and multi-energy performance. Medical Imaging 2014;90331C.
59. Jost G, McDermott M, Gutjahr R, et al. New Contrast Media for K-Edge Imaging With Photon-Counting Detector CT. Invest Radiol 2023;58:515-22.
60. McCollough CH, Leng S, Yu L, et al. Dual- and Multi-Energy CT: Principles, Technical Approaches, and Clinical Applications. Radiology 2015;276:637-53.
61. Mergen V, Racine D, Jungblut L, et al. Virtual Noncontrast Abdominal Imaging with Photon-counting Detector CT. Radiology 2022;305:107-15.
62. Decker JA, Huber A, Senel F, et al. Anemia Detection by Hemoglobin Quantification on Contrast-enhanced Photon-counting CT Data Sets. Radiology 2022;305:650-2.
63. Mergen V, Ghouse S, Sartoretti T, et al. Cardiac Virtual Noncontrast Images for Calcium Quantification with Photon-counting Detector CT. Radiol Cardiothorac Imaging 2023;5:e220307.
64. Sartoretti T, Mergen V, Jungblut L, et al. Liver Iodine Quantification With Photon-Counting Detector CT: Accuracy in an Abdominal Phantom and Feasibility in Patients. Acad Radiol 2023;30:461-9.
65. Mergen V, Sartoretti T, Klotz E, et al. Extracellular Volume Quantification With Cardiac Late Enhancement Scanning Using Dual-Source Photon-Counting Detector CT. Invest Radiol 2022;57:406-11.
66. Symons R, Reich DS, Bagheri M, et al. Photon-Counting Computed Tomography for Vascular Imaging of the Head and Neck: First In Vivo Human Results. Invest Radiol 2018;53:135-42.
67. Leng S, Zhou W, Yu Z, et al. Spectral performance of a whole-body research photon counting detector CT: quantitative accuracy in derived image sets. Phys Med Biol 2017;62:7216-32.
68. Laukamp KR, Lennartz S, Neuhaus VF, et al. CT metal artifacts in patients with total hip replacements: for artifact reduction monoenergetic reconstructions and post-processing algorithms are both efficient but not similar. Eur Radiol 2018;28:4524-33.
69. Higashigaito K, Mergen V, Eberhard M, et al. CT

Angiography of the Aorta Using Photon-counting Detector CT with Reduced Contrast Media Volume. Radiol Cardiothorac Imaging 2023;5:e220140.
70. Euler A, Higashigaito K, Mergen V, et al. High-Pitch Photon-Counting Detector Computed Tomography Angiography of the Aorta: Intraindividual Comparison to Energy-Integrating Detector Computed Tomography at Equal Radiation Dose. Invest Radiol 2022;57:115-21.
71. Nakamura Y, Higaki T, Kondo S, et al. An introduction to photon-counting detector CT (PCD CT) for radiologists. Jpn J Radiol 2023;41:266-82.
72. Yeh BM, FitzGerald PF, Edic PM, et al. Opportunities for new CT contrast agents to maximize the diagnostic potential of emerging spectral CT technologies. Adv Drug Deliv Rev 2017;113:201-22.
73. Kim J, Bar-Ness D, Si-Mohamed S, et al. Assessment of candidate elements for development of spectral photon-counting CT specific contrast agents. Sci Rep 2018;8:12119.
74. Muenzel D, Daerr H, Proksa R, et al. Simultaneous dual-contrast multi-phase liver imaging using spectral photon-counting computed tomography: a proof-of-concept study. Eur Radiol Exp 2017;1:25.
75. Symons R, Cork TE, Lakshmanan MN, et al. Dual-contrast agent photon-counting computed tomography of the heart: initial experience. Int J Cardiovasc Imaging 2017;33:1253-61.
76. Cormode DP, Si-Mohamed S, Bar-Ness D, et al. Multicolor spectral photon-counting computed tomography: in vivo dual contrast imaging with a high count rate scanner. Sci Rep 2017;7:4784.
77. Symons R, Krauss B, Sahbaee P, et al. Photon-counting CT for simultaneous imaging of multiple contrast agents in the abdomen: An in vivo study. Med Phys 2017;44:5120-7.
78. Dangelmaier J, Bar-Ness D, Daerr H, et al. Experimental feasibility of spectral photon-counting computed tomography with two contrast agents for the detection of endoleaks following endovascular aortic repair. Eur Radiol 2018;28:3318-25.
79. Chen ZY, Wang YX, Lin Y, et al. Advance of molecular imaging technology and targeted imaging agent in imaging and therapy. Biomed Res Int 2014;2014:819324.
80. Si-Mohamed S, Cormode DP, Bar-Ness D, et al. Evaluation of spectral photon counting computed tomography K-edge imaging for determination of gold nanoparticle biodistribution in vivo. Nanoscale 2017;9:18246-57.
81. Cormode DP, Roessl E, Thran A, et al. Atherosclerotic plaque composition: analysis with multicolor CT and targeted gold nanoparticles. Radiology 2010;256:774-82.
82. Balegamire J , Vandamme M , Chereul E , et al. Iodinated polymer nanoparticles as contrast agent for spectral photon counting computed tomography. Biomater Sci 2020;8:5715-28.
83. Dong YC, Kumar A, Rosario-Berríos DN, et al. Ytterbium Nanoparticle Contrast Agents for Conventional and Spectral Photon-Counting CT and Their Applications for Hydrogel Imaging. ACS Appl Mater Interfaces 2022;14:39274-84.
84. Barrett JF, Keat N. Artifacts in CT: recognition and avoidance. Radiographics 2004;24:1679-91.
85. Lee CL, Park J, Nam S, et al. Metal artifact reduction and tumor detection using photon-counting multi-energy computed tomography. PLoS One 2021;16:e0247355.
86. Gutjahr R, Halaweish AF, Yu Z, et al. Human Imaging With Photon Counting-Based Computed Tomography at Clinical Dose Levels: Contrast-to-Noise Ratio and Cadaver Studies. Invest Radiol 2016;51:421-9.
87. Si-Mohamed SA, Boccalini S, Lacombe H, et al. Coronary CT Angiography with Photon-counting CT: First-In-Human Results. Radiology 2022;303:303-13.
88. Ahmed Z, Rajendran K, Gong H, et al. Quantitative assessment of motion effects in dual-source dual-energy CT and dual-source photon-counting detector CT. Proc SPIE Int Soc Opt Eng 2022;12031:120311P.
89. Rajiah P, Parakh A, Kay F, et al. Update on Multienergy CT: Physics, Principles, and Applications. Radiographics 2020;40:1284-308.
90. Cammin J, Xu J, Barber WC, et al. A cascaded model of spectral distortions due to spectral response effects and pulse pileup effects in a photon-counting x-ray detector for CT. Med Phys 2014;41:041905.
91. Wang AS, Harrison D, Lobastov V, et al. Pulse pileup statistics for energy discriminating photon counting x-ray detectors. Med Phys 2011;38:4265-75.
92. Ren L, Zheng B, Liu H. Tutorial on X-ray photon counting detector characterization. J Xray Sci Technol 2018;26:1-28.
93. Taguchi K, Frey EC, Wang X, et al. An analytical model of the effects of pulse pileup on the energy spectrum recorded by energy resolved photon counting x-ray detectors. Med Phys 2010;37:3957-69.
94. Flohr T, Schmidt B. Technical Basics and Clinical Benefits of Photon-Counting CT. Invest Radiol 2023;58:441-50.
95. Wildberger JE, Alkadhi H. New Horizons in Vascular

Imaging With Photon-Counting Detector CT. Invest Radiol 2023;58:499-504.
96. Soschynski M, Hagen F, Baumann S, et al. High Temporal Resolution Dual-Source Photon-Counting CT for Coronary Artery Disease: Initial Multicenter Clinical Experience. J Clin Med 2022;11:6003.
97. Hagar MT, Soschynski M, Saffar R, et al. Accuracy of Ultrahigh-Resolution Photon-counting CT for Detecting Coronary Artery Disease in a High-Risk Population. Radiology 2023;307:e223305.
98. Eberhard M, Candreva A, Rajagopal R, et al. Coronary Stenosis Quantification With Ultra-High-Resolution Photon-Counting Detector CT Angiography: Comparison With 3D Quantitative Coronary Angiography. JACC Cardiovasc Imaging 2024;17:342-4.
99. Pinos D, Griffith J 3rd, Emrich T, et al. Intra-individual comparison of image quality of the coronary arteries between photon-counting detector and energy-integrating detector CT systems. Eur J Radiol 2023;166:111008.
100. Yang Y, Fink N, Emrich T, et al. Optimization of Kernel Type and Sharpness Level Improves Objective and Subjective Image Quality for High-Pitch Photon Counting Coronary CT Angiography. Diagnostics (Basel) 2023;13:1937.
101. Kruk M, Noll D, Achenbach S, et al. Impact of coronary artery calcium characteristics on accuracy of CT angiography. JACC Cardiovasc Imaging 2014;7:49-58.
102. Zhang S, Levin DC, Halpern EJ, et al. Accuracy of MDCT in assessing the degree of stenosis caused by calcified coronary artery plaques. AJR Am J Roentgenol 2008;191:1676-83.
103. Mergen V, Sartoretti T, Baer-Beck M, et al. Ultra-High-Resolution Coronary CT Angiography With Photon-Counting Detector CT: Feasibility and Image Characterization. Invest Radiol 2022;57:780-8.
104. Halfmann MC, Bockius S, Emrich T, et al. Ultrahigh-Spatial-Resolution Photon-counting Detector CT Angiography of Coronary Artery Disease for Stenosis Assessment. Radiology 2024;310:e231956.
105. Li Z, Leng S, Halaweish AF, et al. Overcoming calcium blooming and improving the quantification accuracy of percent area luminal stenosis by material decomposition of multi-energy computed tomography datasets. J Med Imaging (Bellingham) 2020;7:053501.
106. Allmendinger T, Nowak T, Flohr T, et al. Photon-Counting Detector CT-Based Vascular Calcium Removal Algorithm: Assessment Using a Cardiac Motion Phantom. Invest Radiol 2022;57:399-405.
107. Mergen V, Rusek S, Civaia F, et al. Virtual calcium removal in calcified coronary arteries with photon-counting detector CT-first in-vivo experience. Front Cardiovasc Med 2024;11:1367463.
108. Nishihara T, Miyoshi T, Nakashima M, et al. Diagnostic improvements of calcium-removal image reconstruction algorithm using photon-counting detector CT for calcified coronary lesions. Eur J Radiol 2024;172:111354.
109. Lo-Kioeng-Shioe MS, Rijlaarsdam-Hermsen D, van Domburg RT, et al. Prognostic value of coronary artery calcium score in symptomatic individuals: A meta-analysis of 34,000 subjects. Int J Cardiol 2020;299:56-62.
110. Rijlaarsdam-Hermsen D, Lo-Kioeng-Shioe MS, Kuijpers D, et al. Prognostic value of the coronary artery calcium score in suspected coronary artery disease: a study of 644 symptomatic patients. Neth Heart J 2020;28:44-50.
111. Hecht H, Blaha MJ, Berman DS, et al. Clinical indications for coronary artery calcium scoring in asymptomatic patients: Expert consensus statement from the Society of Cardiovascular Computed Tomography. J Cardiovasc Comput Tomogr 2017;11:157-68.
112. Agatston AS, Janowitz WR, Hildner FJ, et al. Quantification of coronary artery calcium using ultrafast computed tomography. J Am Coll Cardiol 1990;15:827-32.
113. McCollough CH, Ulzheimer S, Halliburton SS, et al. Coronary artery calcium: a multi-institutional, multimanufacturer international standard for quantification at cardiac CT. Radiology 2007;243:527-38.
114. Blaha MJ, Mortensen MB, Kianoush S, et al. Coronary Artery Calcium Scoring: Is It Time for a Change in Methodology? JACC Cardiovasc Imaging 2017;10:923-37.
115. Pack JD, Xu M, Wang G, et al. Cardiac CT blooming artifacts: clinical significance, root causes and potential solutions. Vis Comput Ind Biomed Art 2022;5:29.
116. van der Werf NR, Si-Mohamed S, Rodesch PA, et al. Coronary calcium scoring potential of large field-of-view spectral photon-counting CT: a phantom study. Eur Radiol 2022;32:152-62.
117. Chang S, Ren L, Tang S, et al. Technical note: Exploring the detectability of coronary calcification using ultra-high-resolution photon-counting-detector CT. Med Phys 2023;50:6836-43.
118. Marsh JF Jr, VanMeter PD, Rajendran K, et al. Ex vivo coronary calcium volume quantification using a high-spatial-resolution clinical photon-counting-detector computed tomography. J Med Imaging (Bellingham) 2023;10:043501.
119. Eberhard M, Mergen V, Higashigaito K, et al. Coronary

Calcium Scoring with First Generation Dual-Source Photon-Counting CT-First Evidence from Phantom and In-Vivo Scans. Diagnostics (Basel) 2021;11:1708.
120. van der Werf NR, Booij R, Greuter MJW, et al. Reproducibility of coronary artery calcium quantification on dual-source CT and dual-source photon-counting CT: a dynamic phantom study. Int J Cardiovasc Imaging 2022;38:1613-9.
121. van der Werf NR, van Gent M, Booij R, et al. Dose Reduction in Coronary Artery Calcium Scoring Using Mono-Energetic Images from Reduced Tube Voltage Dual-Source Photon-Counting CT Data: A Dynamic Phantom Study. Diagnostics (Basel) 2021;11:2192.
122. van der Werf NR, Greuter MJW, Booij R, et al. Coronary calcium scores on dual-source photon-counting computed tomography: an adapted Agatston methodology aimed at radiation dose reduction. Eur Radiol 2022;32:5201-9.
123. van der Werf NR, Rodesch PA, Si-Mohamed S, et al. Improved coronary calcium detection and quantification with low-dose full field-of-view photon-counting CT: a phantom study. Eur Radiol 2022;32:3447-57.
124. Symons R, Sandfort V, Mallek M, et al. Coronary artery calcium scoring with photon-counting CT: first in vivo human experience. Int J Cardiovasc Imaging 2019;35:733-9.
125. Emrich T, Aquino G, Schoepf UJ, et al. Coronary Computed Tomography Angiography-Based Calcium Scoring: In Vitro and In Vivo Validation of a Novel Virtual Noniodine Reconstruction Algorithm on a Clinical, First-Generation Dual-Source Photon Counting-Detector System. Invest Radiol 2022;57:536-43.
126. Nadjiri J, Kaissis G, Meurer F, et al. Accuracy of Calcium Scoring calculated from contrast-enhanced Coronary Computed Tomography Angiography using a dual-layer spectral CT: A comparison of Calcium Scoring from real and virtual non-contrast data. PLoS One 2018;13:e0208588.
127. Fink N, Zsarnoczay E, Schoepf UJ, et al. Impact of Cardiac Motion on coronary artery calcium scoring using a virtual non-iodine algorithm on photon-counting detector CT: a dynamic phantom study. Int J Cardiovasc Imaging 2023;39:2083-92.
128. Burke AP, Farb A, Malcom GT, et al. Coronary risk factors and plaque morphology in men with coronary disease who died suddenly. N Engl J Med 1997;336:1276-82.
129. Virmani R, Burke AP, Farb A, et al. Pathology of the vulnerable plaque. J Am Coll Cardiol 2006;47:C13-8.
130. Koenig W, Khuseyinova N. Biomarkers of atherosclerotic plaque instability and rupture. Arterioscler Thromb Vasc Biol 2007;27:15-26.
131. Virmani R, Kolodgie FD, Burke AP, et al. Lessons from sudden coronary death: a comprehensive morphological classification scheme for atherosclerotic lesions. Arterioscler Thromb Vasc Biol 2000;20:1262-75.
132. Falk E. Pathogenesis of atherosclerosis. J Am Coll Cardiol 2006;47:C7-12.
133. Cau R, Faa G, Nardi V, et al. Long-COVID diagnosis: From diagnostic to advanced AI-driven models. Eur J Radiol 2022;148:110164.
134. Bittner DO, Mayrhofer T, Budoff M, et al. Prognostic Value of Coronary CTA in Stable Chest Pain: CAD-RADS, CAC, and Cardiovascular Events in PROMISE. JACC Cardiovasc Imaging 2020;13:1534-45.
135. Obaid DR, Calvert PA, Gopalan D, et al. Atherosclerotic plaque composition and classification identified by coronary computed tomography: assessment of computed tomography-generated plaque maps compared with virtual histology intravascular ultrasound and histology. Circ Cardiovasc Imaging 2013;6:655-64.
136. Salem AM, Davis J, Gopalan D, et al. Characteristics of conventional high-risk coronary plaques and a novel CT defined thin-cap fibroatheroma in patients undergoing CCTA with stable chest pain. Clin Imaging 2023;101:69-76.
137. Cademartiri F, Balestrieri A, Cau R, et al. Insight from imaging on plaque vulnerability: similarities and differences between coronary and carotid arteries-implications for systemic therapies. Cardiovasc Diagn Ther 2020;10:1150-62.
138. Rotzinger DC, Racine D, Becce F, et al. Performance of Spectral Photon-Counting Coronary CT Angiography and Comparison with Energy-Integrating-Detector CT: Objective Assessment with Model Observer. Diagnostics (Basel) 2021;11:2376.
139. Mergen V, Eberhard M, Manka R, et al. First in-human quantitative plaque characterization with ultra-high resolution coronary photon-counting CT angiography. Front Cardiovasc Med 2022;9:981012.
140. Vattay B, Szilveszter B, Boussoussou M, et al. Impact of virtual monoenergetic levels on coronary plaque volume components using photon-counting computed tomography. Eur Radiol 2023;33:8528-39.
141. Schmidt T, Abbott JD. Coronary Stents: History, Design, and Construction. J Clin Med 2018;7:126.
142. Kim MS, Dean LS. In-stent restenosis. Cardiovasc Ther 2011;29:190-8.
143. Mahnken AH. CT Imaging of Coronary Stents: Past,

Present, and Future. ISRN Cardiol 2012;2012:139823.
144. Gulati M, Levy PD, Mukherjee D, et al. 2021 AHA/ACC/ASE/CHEST/SAEM/SCCT/SCMR Guideline for the Evaluation and Diagnosis of Chest Pain: A Report of the American College of Cardiology/American Heart Association Joint Committee on Clinical Practice Guidelines. Circulation 2021;144:e368-454.
145. Maintz D, Seifarth H, Raupach R, et al. 64-slice multidetector coronary CT angiography: in vitro evaluation of 68 different stents. Eur Radiol 2006;16:818-26.
146. Maintz D, Juergens KU, Wichter T, et al. Imaging of coronary artery stents using multislice computed tomography: in vitro evaluation. Eur Radiol 2003;13:830-5.
147. Mannil M, Hickethier T, von Spiczak J, et al. Photon-Counting CT: High-Resolution Imaging of Coronary Stents. Invest Radiol 2018;53:143-9.
148. Symons R, De Bruecker Y, Roosen J, et al. Quarter-millimeter spectral coronary stent imaging with photon-counting CT: Initial experience. J Cardiovasc Comput Tomogr 2018;12:509-15.
149. Petritsch B, Petri N, Weng AM, et al. Photon-Counting Computed Tomography for Coronary Stent Imaging: In Vitro Evaluation of 28 Coronary Stents. Invest Radiol 2021;56:653-60.
150. Rajagopal JR, Farhadi F, Richards T, et al. Evaluation of Coronary Plaques and Stents with Conventional and Photon-counting CT: Benefits of High-Resolution Photon-counting CT. Radiol Cardiothorac Imaging 2021;3:e210102.
151. Decker JA, O'Doherty J, Schoepf UJ, et al. Stent imaging on a clinical dual-source photon-counting detector CT system-impact of luminal attenuation and sharp kernels on lumen visibility. Eur Radiol 2023;33:2469-77.
152. Koons EK, Thorne JE, Huber NR, et al. Quantifying lumen diameter in coronary artery stents with high-resolution photon counting detector CT and convolutional neural network denoising. Med Phys 2023;50:4173-81.
153. von Spiczak J, Mannil M, Peters B, et al. Photon Counting Computed Tomography With Dedicated Sharp Convolution Kernels: Tapping the Potential of a New Technology for Stent Imaging. Invest Radiol 2018;53:486-94.
154. Michael AE, Schoenbeck D, Becker-Assmann J, et al. Coronary stent imaging in photon counting computed Tomography: Optimization of reconstruction kernels in a phantom. Eur J Radiol 2023;166:110983.
155. Feuerlein S, Roessl E, Proksa R, et al. Multienergy photon-counting K-edge imaging: potential for improved luminal depiction in vascular imaging. Radiology 2008;249:1010-6.
156. Boccalini S, Si-Mohamed SA, Lacombe H, et al. First In-Human Results of Computed Tomography Angiography for Coronary Stent Assessment With a Spectral Photon Counting Computed Tomography. Invest Radiol 2022;57:212-21.
157. Geering L, Sartoretti T, Mergen V, et al. First in-vivo coronary stent imaging with clinical ultra high resolution photon-counting CT. J Cardiovasc Comput Tomogr 2023;17:233-5.
158. Bratke G, Hickethier T, Bar-Ness D, et al. Spectral Photon-Counting Computed Tomography for Coronary Stent Imaging: Evaluation of the Potential Clinical Impact for the Delineation of In-Stent Restenosis. Invest Radiol 2020;55:61-7.
159. Hagar MT, Soschynski M, Saffar R, et al. Ultra-high-resolution photon-counting detector CT in evaluating coronary stent patency: a comparison to invasive coronary angiography. Eur Radiol 2024;34:4273-83.
160. Min JK, Taylor CA, Achenbach S, et al. Noninvasive Fractional Flow Reserve Derived From Coronary CT Angiography: Clinical Data and Scientific Principles. JACC Cardiovasc Imaging 2015;8:1209-22.
161. Rajiah P, Cummings KW, Williamson E, et al. CT Fractional Flow Reserve: A Practical Guide to Application, Interpretation, and Problem Solving. Radiographics 2022;42:340-58.
162. Chen J, Wetzel LH, Pope KL, et al. FFR(CT): Current Status. AJR Am J Roentgenol 2021;216:640-8.
163. Zsarnóczay E, Pinos D, Fink N, et al. Feasibility Of CT-based Fractional Flow Reserve Using A Clinical Photon-Counting Detector CT System. J Cardiovasc Comput Tomogr 2023;17:S80.
164. Brendel JM, Walterspiel J, Hagen F, et al. Coronary artery disease evaluation during transcatheter aortic valve replacement work-up using photon-counting CT and artificial intelligence. Diagn Interv Imaging 2024;105:273-80.
165. Gillies RJ, Kinahan PE, Hricak H. Radiomics: Images Are More than Pictures, They Are Data. Radiology 2016;278:563-77.
166. Mayerhoefer ME, Szomolanyi P, Jirak D, et al. Effects of MRI acquisition parameter variations and protocol heterogeneity on the results of texture analysis and pattern discrimination: an application-oriented study. Med Phys 2009;36:1236-43.
167. Dunning CAS, Rajiah PS, Hsieh SS, et al. Classification

of high-risk coronary plaques using radiomic analysis of multi-energy photon-counting-detector computed tomography (PCD-CT) images. Proc SPIE Int Soc Opt Eng 2023;12465:124652T.
168. Antonopoulos AS, Sanna F, Sabharwal N, et al. Detecting human coronary inflammation by imaging perivascular fat. Sci Transl Med 2017;9:eaal2658.
169. Goeller M, Tamarappoo BK, Kwan AC, et al. Relationship between changes in pericoronary adipose tissue attenuation and coronary plaque burden quantified from coronary computed tomography angiography. Eur Heart J Cardiovasc Imaging 2019;20:636-43.
170. Hoshino M, Yang S, Sugiyama T, et al. Peri-coronary inflammation is associated with findings on coronary computed tomography angiography and fractional flow reserve. J Cardiovasc Comput Tomogr 2020;14:483-9.
171. Yuvaraj J, Lin A, Nerlekar N, et al. Pericoronary Adipose Tissue Attenuation Is Associated with High-Risk Plaque and Subsequent Acute Coronary Syndrome in Patients with Stable Coronary Artery Disease. Cells 2021;10:1143.
172. Chen X, Dang Y, Hu H, et al. Pericoronary adipose tissue attenuation assessed by dual-layer spectral detector computed tomography is a sensitive imaging marker of high-risk plaques. Quant Imaging Med Surg 2021;11:2093-103.
173. Oikonomou EK, Marwan M, Desai MY, et al. Non-invasive detection of coronary inflammation using computed tomography and prediction of residual cardiovascular risk (the CRISP CT study): a post-hoc analysis of prospective outcome data. Lancet 2018;392:929-39.
174. Goeller M, Achenbach S, Herrmann N, et al. Pericoronary adipose tissue CT attenuation and its association with serum levels of atherosclerosis-relevant inflammatory mediators, coronary calcification and major adverse cardiac events. J Cardiovasc Comput Tomogr 2021;15:449-54.
175. Hoshino M, Zhang J, Sugiyama T, et al. Prognostic value of pericoronary inflammation and unsupervised machine-learning-defined phenotypic clustering of CT angiographic findings. Int J Cardiol 2021;333:226-32.
176. Mergen V, Ried E, Allmendinger T, et al. Epicardial Adipose Tissue Attenuation and Fat Attenuation Index: Phantom Study and In Vivo Measurements With Photon-Counting Detector CT. AJR Am J Roentgenol 2022;218:822-9.

Cite this article as: Meloni A, Maffei E, Positano V, Clemente A, De Gori C, Berti S, La Grutta L, Saba L, Bossone E, Mantini C, Cavaliere C, Punzo B, Celi S, Cademartiri F. Technical principles, benefits, challenges, and applications of photon counting computed tomography in coronary imaging: a narrative review. Cardiovasc Diagn Ther 2024;14(4):698-724. doi: 10.21037/cdt-24-52

